GENERAL ELECTRIC

GENERAL ELECTRIC COMPANY
CORPORATE RESEARCH AND DEVELOPMENT
Schenectady, N.Y.

OXIDE CERAMIC LASER

ANNUAL TECHNICAL REPORT (ITEM 0002-A002)

Program Code No.:	02D10K71
Contract No.:	N00014-70-C-0360
Principal Investigator:	Charles D. Greskovich (516) 346-8771 Ext. 6122
Contractor:	General Electric Company
Effective Date:	June 1, 1970
Expiration Date:	May 31, 1973
Amount of Contract:	$297,398.00

July 24, 1972

Scientific Officer:	A. M. Diness, Code 471 Office of Naval Research Arlington, Va. 22217

Sponsored By

Advanced Research Projects Agency
ARPA Order No. 1587, Amend. #3

SEE AD736223

The views and conclusions contained in this document are those of the author and should not be interpreted as necessarily representing the official policies, either expressed or implied, of the Advanced Research Projects Agency or the U.S. Government.

This research was supported by the Advanced Research Projects Agency of the Department of Defense and was monitored by ONR under Contract No. N00014-70-C-0360.

62

UNCLASSIFIED

Security Classification

DOCUMENT CONTROL DATA - R & D

(Security classification of title, body of abstract and indexing annotation must be entered when the overall report is classified)

1 ORIGINATING ACTIVITY (Corporate author)
General Electric Company
Corporate Research & Development
Post Office Box 8
Schenectady, New York 12301

2a. REPORT SECURITY CLASSIFICATION
Unclassified

2b. GROUP

3 REPORT TITLE

OXIDE CERAMIC LASER

4 DESCRIPTIVE NOTES (Type of report and inclusive dates)
Annual Technical Report, June 1, 1971, through May 31, 1972

5. AUTHOR(S) (First name, middle initial, last name)

Charles D. Greskovich

6 REPORT DATE	7a. TOTAL NO OF PAGES	7b. NO OF REFS
July 24, 1972	49	12

8a. CONTRACT OR GRANT NO	9a. ORIGINATOR'S REPORT NUMBER(S)
N00014-70-C-0360	SRD-72-105
b. PROJECT NO. ARPA Order #1587 Amend. #3	
c. 02D10K71	9b. OTHER REPORT NO(S) (Any other numbers that may be assigned this report)
d.	

10. DISTRIBUTION STATEMENT

11. SUPPLEMENTARY NOTES	12 SPONSORING MILITARY ACTIVITY
	Advanced Research Projects Agency 1400 Wilson Boulevard Arlington, Virginia 22209

13. ABSTRACT

Porosities as low as 10^{-6} to 10^{-7} are attained in neodymium-doped Yttralox (NDY) ceramics, provided that pore densities for large pores are low and that pore cluster formation is prevented during sintering. Large pores ($\approx 50\mu$) found in sintered material prepared from ball-milled powder originates from particles of mill-lining introduced into the powder batch during milling. The origin of pore clusters is caused by large Yttralox chips that fragment off of the Yttralox cylinders during milling and act as nuclei for discontinuous grain growth during sintering. NDY ceramics of high optical quality can be produced by an oxalate powder preparation technique combined with a sintering process. The most common scattering defects observed microscopically are pores, solid second phase which can be eliminated in most cases, and orange peel. Submicroscopic scattering centers probably exist in NDY rods cooled slowly from the sintering temperature. A laser rod cooled rapidly has a laser threshold of 8 joules at 95% output mirror reflectivity, an active loss coefficient of 2.6%/cm, and a slope efficiency of 0.19%. Laser glass (OI,ED2) for the same tests exhibits a threshold of 9 joules, an active loss coefficient of 0.76%/cm, and a slope efficiency of 0.44%. Neodymium-doped Yttralox ceramic now has as lasing efficiency approximately 43% of laser glass.

1a

Details of illustrations in this document may be better studied on microfiche

DD FORM 1 NOV 1473

UNCLASSIFIED

Security Classification

14 KEY WORDS	LINK A		LINK B		LINK C	
	ROLE	WT	ROLE	WT	ROLE	WT
Nd-doped Yttralox lasers						
Ceramic Processing						
Sintering						
Grain Growth						
Pores						
Spectral Transmittance						
Laser Threshold and Efficiency						
Scattering Centers						

12

- TABLE OF CONTENTS -

FOREWORD

This research was sponsored by Advanced Research Projects Agency and carried out in the Metallurgy and Ceramics Laboratory and the General Physics Laboratory of the General Electric Company Corporate Research and Development under U.S. Navy Contract N00014-70-C-0360 entitled "Oxide Ceramic Laser".

This work was administered under the direction of Dr. Arthur Diness from June 1, 1971, to May 31, 1972.

The author acknowledges the contributions of the following individuals to the Program:

- J. E. Burke, for helpful guidance during this program:
- J. C. Almasi and J. P. Chernoch, for active and passive optical measurements:
- C. O'Clair, for ceramic processing procedures and heat treatments.

- ABSTRACT -

Porosities as low as 10^{-6} to 10^{-7} are attained in neodymium-doped Yttralox (NDY) ceramics, provided that pore densities for large pores are low and that pore cluster formation is prevented during sintering. Large pores ($\approx 50\mu$) found in sintered material prepared from ball-milled powder originates from particles of mill-lining introduced into the powder batch during milling. The origin of pore clusters is caused by large Yttralox chips that fragment off of the Yttralox cylinders during milling, mix into the fine powder particles ($\approx 0.1\mu$) and act as nuclei for discontinuous grain growth during sintering.

The kinetics of removal of pores entrapped inside grains during the late stages of sintering are found to be related directly to the amount of grain growth. In this stage of sintering, the mechanism of pore elimination is due to migrating grain boundaries on which pores shrink rapidly. These experimental findings, in conjunction with theoretical calculations, strongly indicate that pore shrinkage does not occur by a typical volume diffusion mechanism but, most likely, by a grain-boundary diffusion mechanism.

Grain growth during final stages of sintering of NDY material prepared from milled powder approximately follows as $t^{1/3}$ behavior, whereas grain growth approximately follows a $t^{1/2}$ law in unmilled material at 2000°C. The mechanism of grain growth in the milled material may be related to inhibition of grain boundary movement by sulfur-rich, second-phase particles; the mechanism of grain growth in unmilled material may be an impurity drag effect.

Abstract (continued)

NDY ceramics of high optical quality can be produced by an oxalate powder preparation technique combined with a sintering process. Twymann Green interforometer patterns show that the optical quality of NDY rods is almost comparable to that of a single crystal rod of Nd-doped yttrium aluminum garnet but not as good as that of laser glass. Spectral transmittance of Nd-free Yttralox, including surface reflection losses, is greater than 80% between 3/4 and 6μ for a 3-1/2 mm thick plate. Large-angle scattering losses measured by passive laser testing appears not to be a reliably quick method of distinguishing NDY rods of good and poor optical quality.

Active laser measurements (laser threshold energy, active loss coefficient, and lasing slope efficiency) can assess the optical quality of NDY laser rods. The most common scattering defects observed microscopically are pores, solid second phase which can be eliminated in most cases, and orange peel (a point-to-point variation in refractive index). Submicroscopic scattering centers probably exist in NDY rods cooled slowly from the sintering temperature because there is a large improvement in the optical quality of the same rod when cooled rapidly from the sintering temperature. A laser rod cooled rapidly has a laser threshold of 8 joules at 95% output mirror reflectivity, an active loss coefficient of 2.6%/cm, and a slope efficiency of 0.19%. Laser glass (OI,ED2) for the same tests exhibits a threshold of 9 joules, an active loss coefficient of 0.76%/cm, and a slope efficiency of 0.44%. Neodymium-doped Yttralox ceramic now has a lasing efficiency approximately 43% of laser glass.

- LIST OF ILLUSTRATIONS -

List of Illustrations (continued)

List of Illustrations (continued)-

List of Illustrations (continued)

- LIST OF TABLES -

I. INTRODUCTION

The capability of generating laser radiation having both high-peak power and high-average power is important for the future development of high-speed tracking and illuminating devices for military applications. In the neodymium (Nd^{3+}) wavelength region of about 1.06μ, the two conventional laser materials considered for these applications are Yttrium Aluminum Garnet (YAG) and glasses. Single-crystal YAG exhibits high-average power because of its high thermal conductivity but low-peak power because of its high gain; i.e., narrow, stimulated-emmision linewidth. The tedious growth of YAG single crystals introduces the further disadvantages of high cost and limited size. The glass laser can produce high-peak power because of its low gain but low-average power because of its poor thermal conductivity. Using conventional rod design, high-peak power at high-average power cannot be easily achieved with either neodymium-doped YAG or glasses.

Neodymium-doped Yttralox® ceramic is a polycrystalline, cubic material made from a solid solution of 89 mole % Y_2O_3, 10% ThO_2, and 1% Nd_2O_3 and can be produced with excellent optical quality by the conventional technique of cold-pressing and sintering. During the first year of the present contract, 7.6 cm x 0.5 cm rods were synthesized with residual porosities between 10^{-5} to 10^{-7} and exhibited lasing behavior. This ceramic is promising as an efficient laser and a high-power infrared window material provided that the optical loss coefficient is very low. Nd-doped Yttralox (NDY) ceramic is attractive as an intermediate gain, solid-state laser material because it has a broader stimulated-emission linewidth then that of YAG and a higher thermal conductivity than that of glass.

Processing developments during the first year's contract indicated that the oxalate powder preparation technique combined with a sintering process is a promising way of producing laser quality optical material.

I. Introduction (continued)

This process consists of dissolving appropriate amounts of yttrium, thorium, and neodymium nitrates with purities of 99.99, 99.9, and 99.999%, respectively, into deionized water. This salt solution is filtered and dripped into a filtered solution of oxalic acid which is 80% saturated at room temperature and contains 100% excess oxalic acid required to convert the nitrates into oxalates. During precipitation, the oxalic acid bath is continuously stirred with a Teflon-coated, magnetic stirring bar. After precipitation, the oxalate precipitate is stirred vigorously, washed with filtered deionized water to remove residual acid, vacuum filtered, dehydrated at 110°C for 24 hours, and calcined for four hours at 800°C in flowing air (3 SCFH). The calcined powder is dry-milled for 6 hours with 1 wt.% stearic acid in a rubber-lined ball mill (volume = 1.2ℓ) that contains ThO_2-doped Y_2O_3 cylinders as a grinding medium. After milling, the particles are of the order of 0.1μ or less in size. Compacts are formed from the milled powder by isostatically pressing at 38k psi and are given an oxidation treatment in air at 1100°C for 2 hours to remove stearic acid and rubber particles. Specimens prepared from milled or unmilled calcined powder are sintered at 2170°C for various times in a dry hydrogen atmosphere and cooled to room temperature in approximately 6 hours in wet hydrogen.

Although the ultimate goal of the current contract is to produce an efficient NDY laser or a high-power infrared window material, major effort is being devoted towards generating an understanding of the origin of optical defects or inhomogeneities and ways to eliminate or minimize them in sintered ceramics. The overall objectives are to:

(1) develop a process to reproducibly fabricate ultra-clear NDY material comprised of the composition mentioned;

(2) understand the origin of pores, second phases, and other light-scattering defects, mechanisms of their removal, and methods to determine their concentration, shape, and size distribution in laser quality material; and,

I. Introduction (continued)

(3) determine the lasing quality of NDY and the interrelationships between optical quality, microstructure, and ceramic processing.

II. POROSITY

A. Large Pores

Sintered NDY ceramic prepared from either "as calcined" powder or from ball-milled powder contains, in general, an occasional large pore greater than 50μ in size. Such large pores contribute greatly to light scattering losses because for pores much larger than the wavelength, the total scattering cross-section is equal to twice its geometrical cross section, $2\pi r^2$. In addition, large pores have small average curvatures and low driving forces for shrinkage. The elimination of these large pores is virtually impossible under practical conditions of isothermal sintering.

A large pore occasionally found in sintered material prepared from unmilled, calcined powder is shown in Figure 1. A galaxy of small pores surround the large one. In order to determine if the origin of these pores are caused by incomplete decomposition of the starting oxalate powder (800°C for 4 hour in air), the calcination temperature was increased to 850°C. Sintered specimens prepared from this powder contained fewer large pores greater than 50μ in size. Apparently, the higher calcination temperature more completely decomposed the Y-Th-Nd oxalate to the respective oxides and minimized the formation of large pores originating from a region that contained incompletely decomposed material. The high density of small pores located in the vicinity of the large one are stabilized probably by entrapped CO and CO_2 gases.

The morphology and size of large pores found in sintered material prepared from ball-milled powder appears to depend on the type of mill

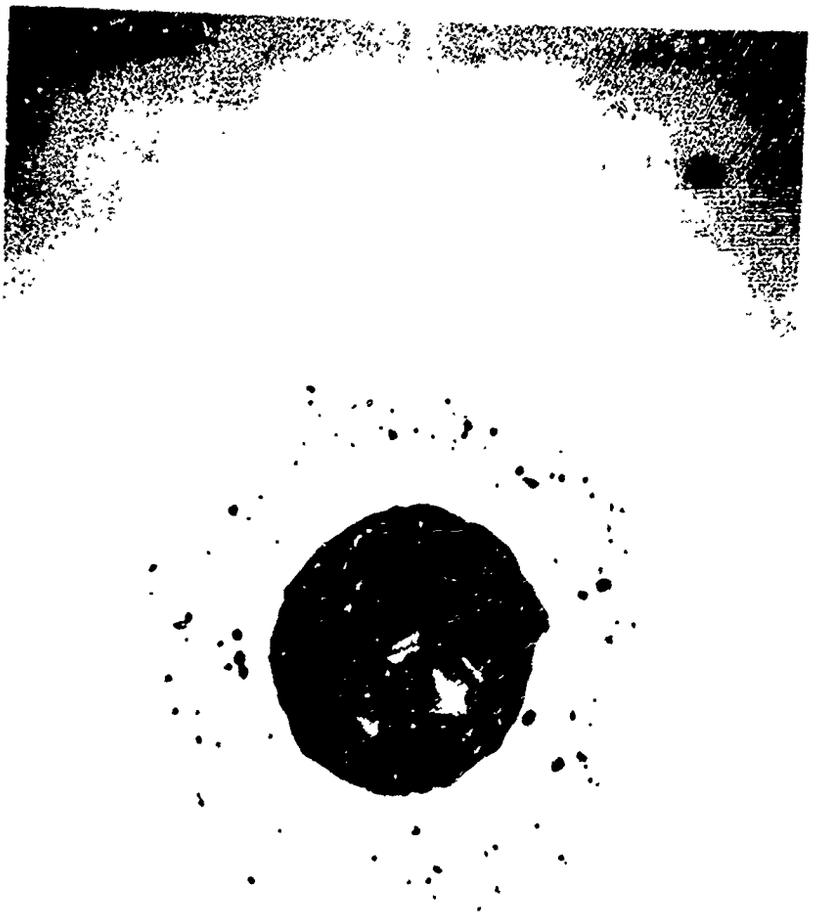

Figure 1 Galaxy of small pores stabilized in the vicinity of a large pore. Transmitted light, 210X.

A. Large Pores (continued)

lining. Typical photomicrographs of large pores found in sintered material prepared from powder milled for 6 hours in rubber-lined and polyurethane-lined mills are shown in Figures 2 and 3, respectively. Many large pores are located at grain boundaries (Figure 4). In several instances, a particle of rubber and polyurethane in milled powders has been observed with the naked eye. The tubular-shaped pores illustrated in Figure 3 originate most likely from excessive abrasion of the polyurethane lining. Since polyurethane lining supposedly has the greatest abrasion resistance of any synthetic rubber, the large pore shown in Figure 2 is thought also to be caused by a rubber particle. Further support for the above conclusion can be deduced from preliminary milling experiments in which the surface roughness of the grinding medium was changed for the same weight of medium. Results show that the use of rough cylinders gives rise to a high density of large pores in the sintered product, indicating a higher coefficient of friction between the rough cylinders and the mill lining.

B. Small Pores

The majority of pores observed in all sintered material are less than 5μ in size (see quantitative-pore data below) and are usually located inside grains that are of the order of 100μ in size. These pores undoubtedly originate from the pore size distribution in the green compact and from changes in this distribution as a function of sintering time at temperature. Although the total pore density in most sintered specimens is of the order of 20,000 to 100,000/cm^3, the probability of intersecting a few pores in a random section through the material is very low. The entrapment of small pores inside growing grains occurs during continuous grain growth in powder compacts prepared from unmilled powder (see grain growth kinetics, below). Although it is not exactly known at what stage of the sintering and grain growth processes these pores become engulfed, once the velocity of a grain boundary exceeds

Figure 2 Large pore in sintered material prepared from powder milled in a rubber-lined mill. Sintered 60 hours at 2170°C. Transmitted light, 270X.

Figure 3 Large tubular-shaped pore in sintered material prepared from powder milled in a polyurethane-lined mill. Sintered 60 hours at 2170°C. Transmitted light, 240X.

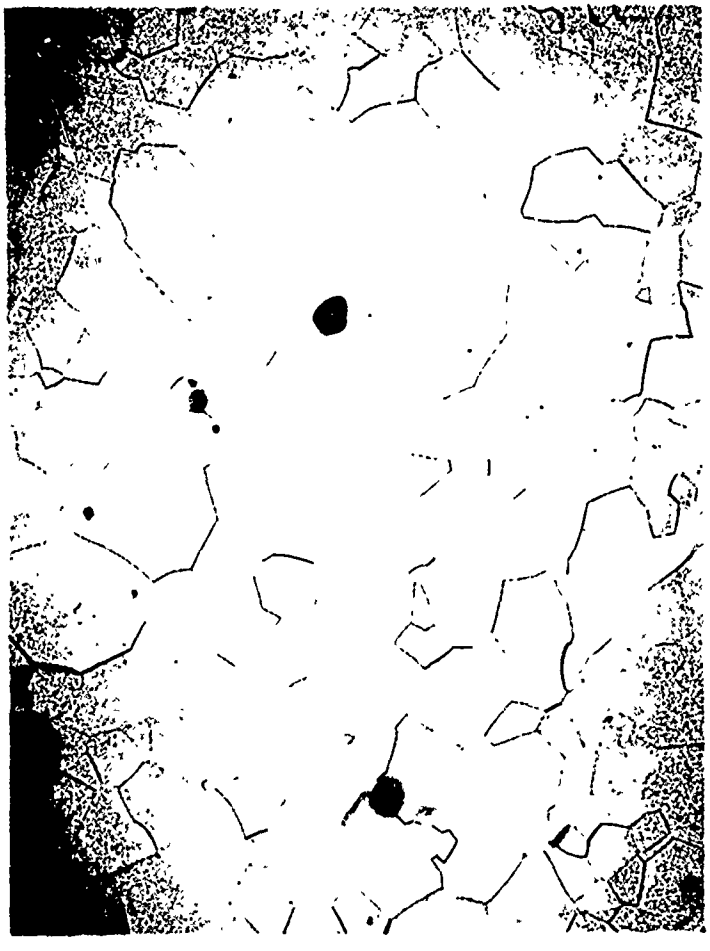

Figure 4 Large pores located at grain boundaries in sintered material prepared from powder milled in a polyurethane-lined mill. Sintered 60 hours at 2170°C. Reflected light, 75X.

B. Small Pores (continued)

that of the pore on the boundary, the pore becomes occluded in the growing grain. The shrinkage rate of entrapped pores is experimentally found to be very low because there is a small flux of vacancies from the pore surface (vacancy source) to the grain boundaries (vacancy sink).

C. Pore Clusters

During the first six months of this year's contract, sintered NDY specimens prepared from ball-milled powder contained an unusually large number of pore clusters that were distributed throughout the bulk of the material. Prior to this time, sintered material contained very few pore clusters when prepared by the identical process. Transmitted-light photomicrographs of various pore clusters are shown in Figures 5 and 6. Individual pores in a cluster were approximately 5μ or less in size and varied in number. In a few cases, over 100 pores have been observed in a given pore cluster. A typical pore cluster density commonly observed was approximately $30/mm^3$.

An extensive investigation of the origin of pore cluster formation in sintered NDY ceramics was obviously in order, especially since, from the author's experience, such pore clusters are frequently found in other polycrystalline ceramics with high optical quality, such as MgO-doped Al_2O_3 and Y_2O_3-doped ThO_2. This study resulted in the following experimental findings:

1. Sintered material made from unmilled, calcined powder contained very few pore clusters whereas that made from dry-milled, calcined powder always contained numerous pore clusters.
2. Changing the weight ratio of grinding medium to powder charge in the rubber-lined mill from 24:1 to 20:1 had no major effect on cluster formation.
3. The dry-milling of NDY powder with 1 wt.% stearic acid in rubber-lined, neoprene-lined and polyurethane-lined mills yielded sintered material having many pore clusters.

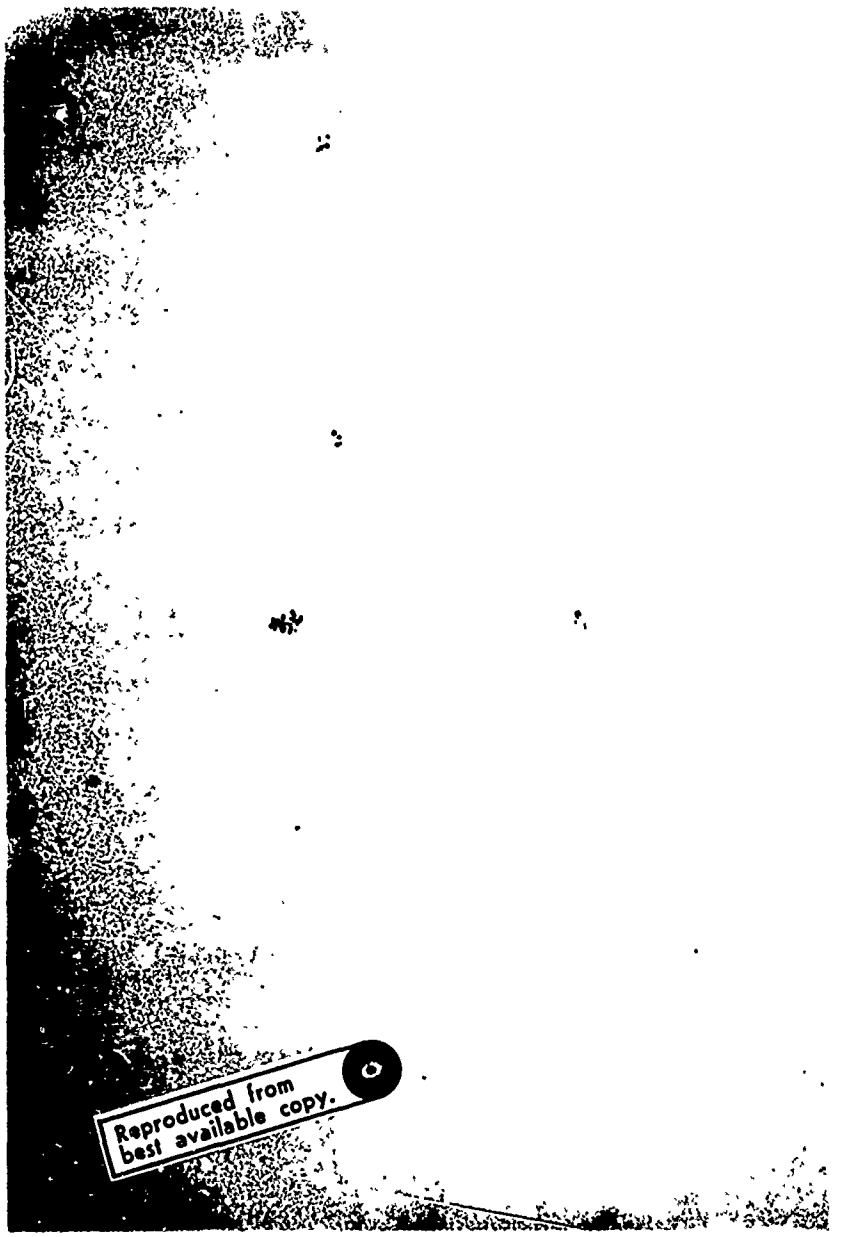

Figure 5 Pore clusters in NDY ceramics prepared from powder ball-milled in a rubber lined mill. Sintered 34 hours at 2170°C. Transmitted light, 600X.

Figure 6 Large pore cluster in NDY ceramic prepared from powder ball-milled in a rubber lined mill. Sintered 34 hours at 2170°C. Transmitted light, 600X.

C. Pore Clusters (continued)

4. The dry-milling of NDY powder in the absence of stearic acid and the dry-milling of neodymium-free Yttralox powder also yielded material characterized by pore cluster formation.
5. Pore clusters did not originate from contamination caused by the furnace atmosphere prevailing during the oxidation treatment at 1100°C, a processing step used only for compacts prepared from milled powder.

It was clear from these experimental observations that pore cluster formation originated during the ball-milling operation and that their elimination was not influenced by the weight ratio of grinding medium to powder charge, different ball-mill linings, absence of stearic acid, furnace atmosphere present during the oxidation step, and presence of the neodymium additive.

A close examination of the Yttralox cylinders used for the ball-milling experiments revealed that there was excessive wear at various locations on their surfaces. This was an indication that large chips had fragmented off of the cylinders during milling, mixed into the fine powder (0.1μ) batch, and acted as nuclei for discontinuous grain growth during sintering. Large chips are possible because the average grain size of the cylinders was approximately 100μ. By removing the most severely abraded cylinders by visual inspection and proceeding with a typical milling experiment, the number of pore clusters in the sintered material was drastically reduced to about 2 per mm^3 of solid. The use of the same cylinders during milling, after they had a fire polish at high temperature, also produced sintered material with essentially no pore clusters. There was a tremendous increase in the number of pore clusters by roughening the surfaces of the fire-polished cylinders by first wet-grinding and then subsequently using these cylinders in a typical dry-milling experiment.

C. Pore Clusters (continued)

Two additional experiments were performed to establish [illegible]cally the origin of pore clusters in NDY ceramics. Fine grain size ($\approx 1.5\mu$) Yttralox cylinders were synthesized to increase the strength of the cylinders and eliminate the source of large-size chips or fragments. The use of these fine-grained cylinders in the standard dry-milling step resulted in sintered material that contained less than 1 pore cluster per mm^3 of solid analyzed. If pore clusters were indeed caused by fragments much larger than the powder particles, then the intentional addition of coarse particles into the mill charge should cause the return of pore clusters in the sintered material. The addition of 0.5 wt.% of -40 mesh ($\approx 420\mu$) NDY particles to the mill charge did produce over 200 pore clusters per mm^3 of sintered material.

The consequence of a markedly mixed particle size in the starting powder gives rise to a condition for discontinuous grain growth during sintering of the powder compact. The site of a large particle is a discontinuous grain growth nucleus. During the early stages of sintering, discontinuous grain growth occurs and the grain boundaries developed at the interfaces between the large and small grains move on across pores and reform on the other side. If this mechanism is operating, then pores should be entrapped inside the rapidly growing grains. That such is the case can be seen in transmitted light photomicrographs illustrated in Figures 7 and 8. Although the use of polished sections and reflected light microscopy cannot, in general, reveal pore clusters in a sintered specimen containing a small cluster concentration, this technique can show clusters very clearly when there is a large concentration due to the intentional addition of coarse particles into the fine powder in the milling step (Figure 9). On the other hand, transmitted light microscopy can reveal the morphology and location of small concentrations of pore clusters when used in combination with sintered specimens having surface grain anisotropy caused by rough

Figure 7 Pore cluster located inside a large grain having 11 sides (in cross-section). Grain boundaries revealed by surface grain anisotropy caused by rough polishing. Transmitted light, 240X.

Figure 8 Pore cluster located inside a large grain whose boundaries are revealed by grain-boundary decoration. Specimen sintered 11 hours at 2115°C. Transmitted light, 240X.

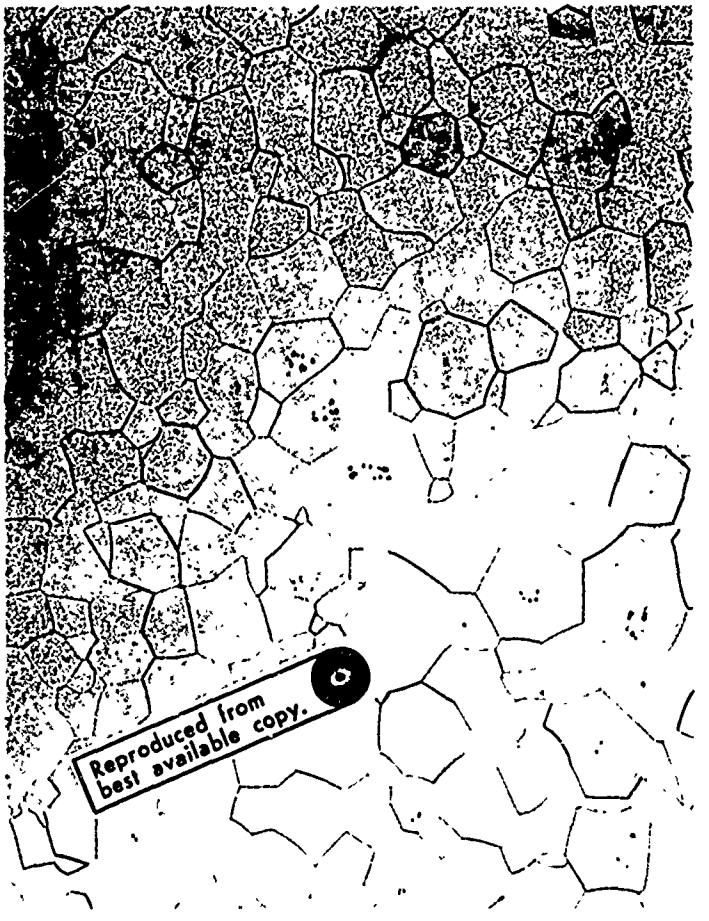

Figure 9 Pore clusters, having several morphologies, located inside grains. Specimens sintered for 16 1/2 hours at 2160°C. Reflected light, 100X.

C. Pore Clusters (continued)

polishing (Figure 7) and specimens containing a sulfur-rich phase which decorates the grain boundaries (Figure 8).

It has been demonstrated, then, that the origin and mechanism of pore cluster formation in NDY ceramics (and most likely in other sintered ceramics) is caused by a very broad particle size distribution in the powder compact. Large particles in the distribution can arise from the abrasion of large grain size cylinders or balls used for ball-milling the powder or from the normal spread in the size distribution obtained by the powder particles during powder synthesis or milling. The elimination of pore cluster formation is essential to the production of sintered material with low porosity and high optical quality because, as stated above, pores shrink much more slowly when they are located off of, rather than on, grain boundaries. In the present case, fine-grained (1.5μ) Yttralox cylinders will be used in future milling experiments.

D. Quantitative Pore Measurements

The quantitative determination of porosity or the volume fraction of pores in sintered rods of good optical quality was easily accomplished with a petrographic microscope, using a ruled graticule and transmitted white light. The technique involved using a magnification of X285, scanning through known cylindrical solid volumes, and counting the number of pores and measuring their average size. Pores less than 0.5μ could not be resolved at that magnification. Pore volumes in various size ranges were then calculated and normalized to the total scanned solid volume. In general, between 1 and 3 mm^3 of solid was analyzed in the specimens described below.

Measurements of pore-size frequency-distribution were made in three rods, YTC 12-1, YTC 13-4, YTC 16-3, that were processed identically but

D. Quantitative Pore Measurements (continued)

at different times during the past 18 months. (The exact processing procedure has been described in the introduction section of this report.) The pore-size frequency-distributions in these specimens are given in Figures 10, 11, and 12. The majority of pores are, in general, less than 5μ in size with a peak in the distribution between 1 and 2.5μ. Even though there are only a few pores greater than 10μ, these pores contribute greatly to residual porosity. This can be seen by comparing the distribution of pore density versus pore size and the residual porosity in Figures 10 and 11. Porosities as low as 10^{-6} to 10^{-7} can be attained, provided that pore densities for large pores are very low and that pore cluster formation can be prevented during sintering. The pore data represented in Figure 12 was taken from a specimen in which pores were primarily in the form of pore clusters. In fact, specimen YTC 16-3 contained approximately 38 pore clusters/mm^3, a pore cluster being defined as a pore group containing three or more pores. Over the same pore-size range, pore densities found in YTC 16-3 are more than an order of magnitude higher than those found in YTC 12-1 and YTC 13-4 specimens which contain very few pore clusters. As a result of the presence of a large number of pore clusters, specimen YTC 16-3 had a porosity of about 1.2×10^{-5}.

It has been observed that pores can be distributed uniformly and non-uniformly throughout a sintered disk or rod. A non-uniform distribution of porosity was definitely observed in YTC 13-4 rod in which the pore density near the surface region was approximately an order of magnitude higher than that near the center region of the rod. An explanation of this observation is not presently known, but it is thought that such a pore arrangement may be caused by either agglomerate and rubber particle migration during powder compaction or pore migration up a temperature gradient created during heating to the sintering temperature. In a transparent material, a uniform distribution of pores, as well as a

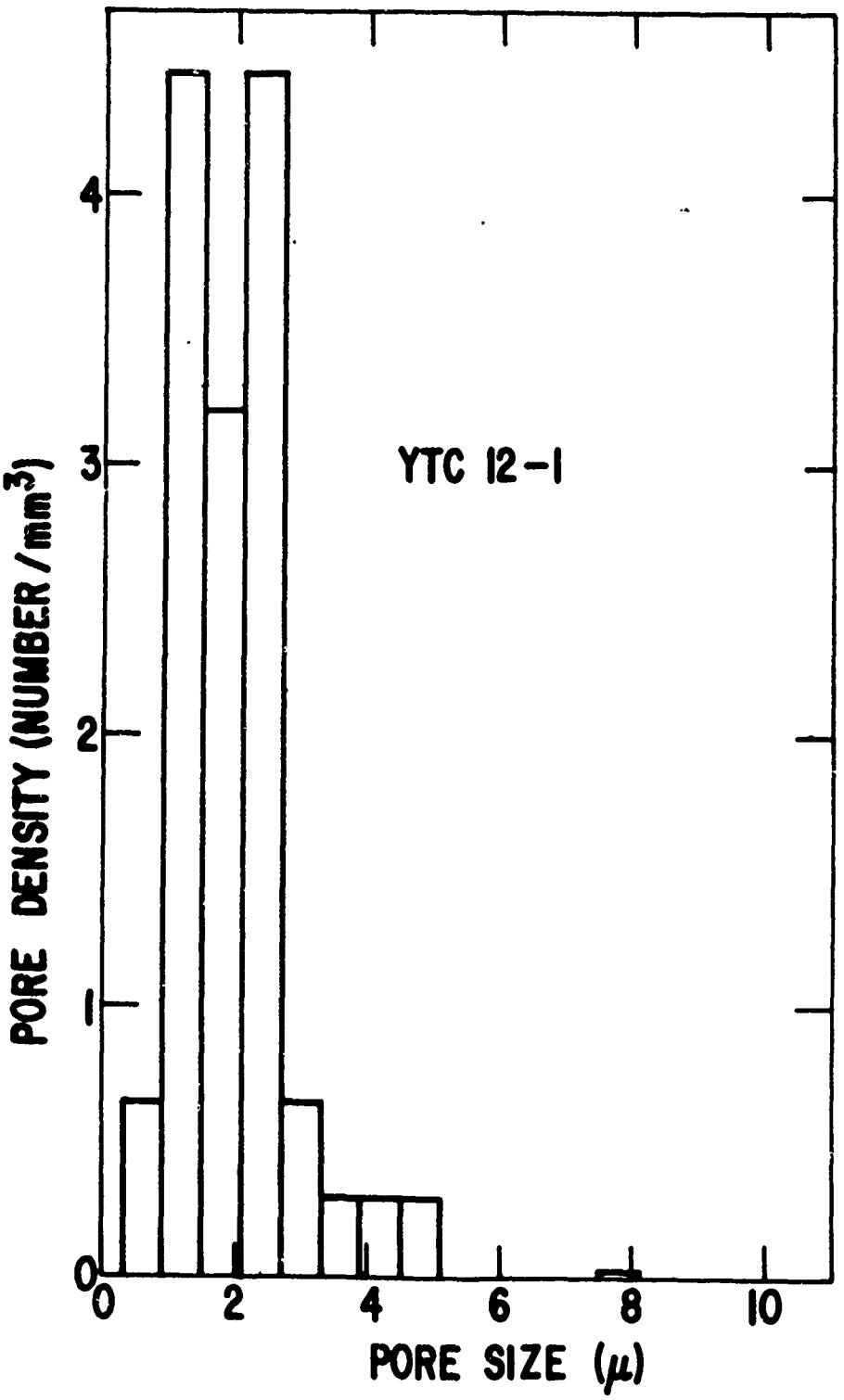

Figure 10 Pore density versus pore size for YTC12-1 rod. Sintered 125 hours at 2170°C.

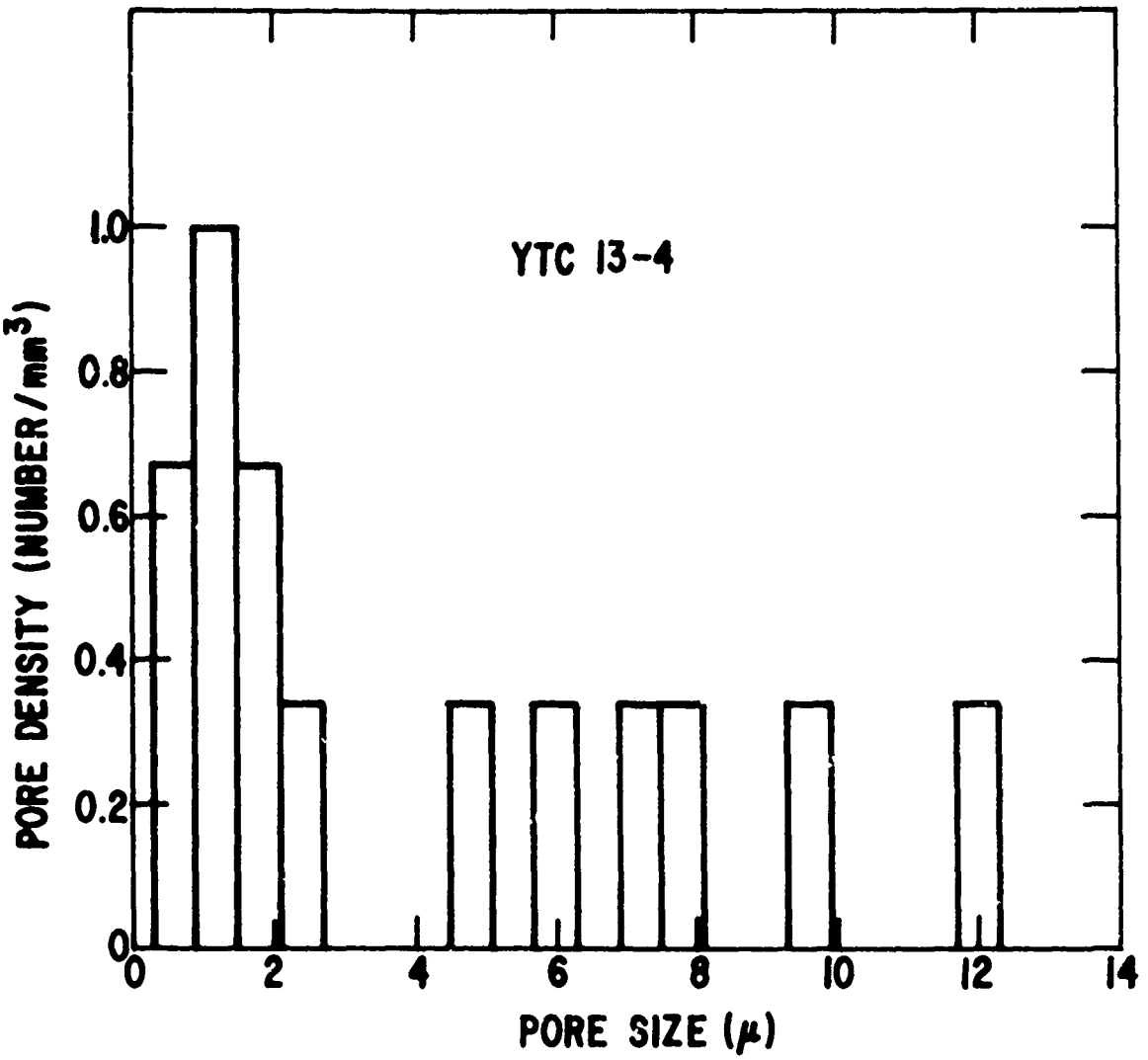

Figure 11 Pore density versus pore size for YTC 13-4 rod sintered 58 hours at 2150°C.

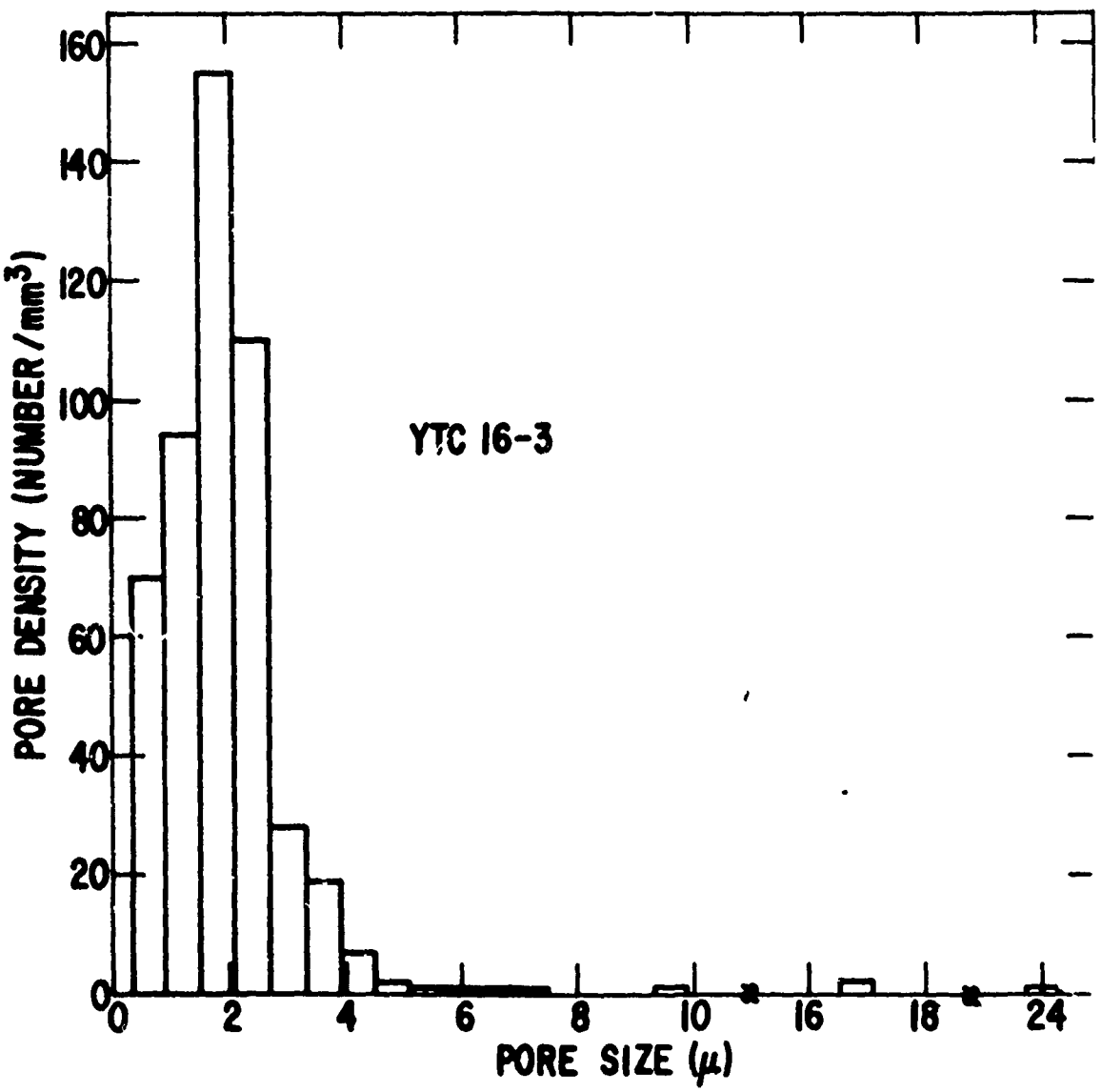

Figure 12 Pore density versus pore size for YTC16-3 rod sintered 90 hours at 2170° C.

D. Quantitative Pore Measurements (continued)

uniform microstructure in general, is desirable because it lends itself to a simpler interpretation of physical property measurements, such as light-scattering effects.

E. Kinetics of Pore Disappearance During the Late Stages of Sintering

It is generally accepted that pore removal during the late stages of sintering is diffusion controlled and that closed pores shrink by the transport of vacancies and soluble gas atoms from them to the grain boundaries.[1] Furthermore, it is usually assumed that the direct flow of the rate-limiting species, which is usually presumed to be the entrapped gas, into a grain boundary along its interesection with a pore is negligible compared to the flow resulting from volume diffusion from the surface of the pore. In the very late stages of sintering in which the volume fraction of pores is of the order of 10^{-4} or less, pore-grain boundary interactions control sintering and pore-pore interactions are virtually minimized. The study of pore elimination in this regime of sintering offers the opportunity to make some deductions about the mechanism of pore shrinkage.

Several measurements of pore size frequency distribution were made on the same NDY sample during the course of prolonged heating at 2170°C in dry hydrogen. This material, prepared from ball-milled powder, is well-suited to the study of final stages of sintering because of its low pore density and high transparency. At the time the first measurements were made, after 33 hours at temperature, the average pore density was less than 1 per grain. The pore distribution was such that a few pores or a pore cluster were located inside an appreciable number of grains.

The data were obtained by measuring between 130 and 750 pores in about 0.75 to 3 mm^3 of solid and are shown in Figure 13. The pore-size

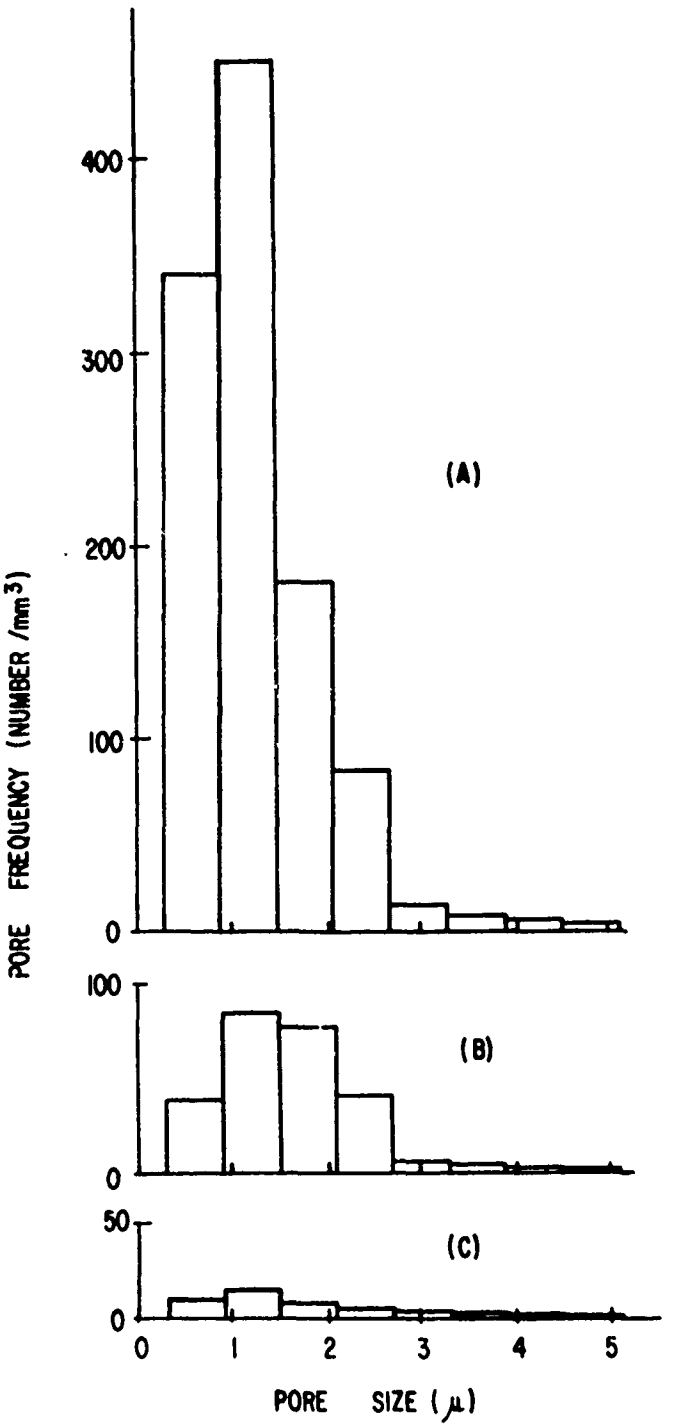

Figure 13 Pore density versus pore size for a specimen sintered at 2170°C. (A) Specimen sintered 33 hours and characterized by a grain size (D_g) of 110μ and a volume fraction of pores (V_f) of 2.3×10^{-6}. (B) Specimen sintered 91 hours, having $D_g = 190\mu$ and $V_f = 8.7 \times 10^{-7}$. (C) Specimen sintered 180 hours, having $D_g = 260\mu$ and $V_f = 2.5 \times 10^{-7}$.

E. Kinetics of Pore Disappearance...(continued)

distribution is seen to remain essentially unchanged, whereas the pore density decreases with time of heating. Thus, it appears that pores are disappearing from the sample but that the pores observed at any time have not shrunk appreciably. This anomaly can be resolved by considering the grain growth that occurred during the experiment. The grain growth data are shown in Figure 15 (see later).

During the heating from 33 to 91 to 180 hours, the average grain size increased in the ratio 1:1.73:2.36, respectively. On the average, then, the volume occupied by about 5.2 grains at 33 hours contained one grain after 91 hours. Similarly, about 13.3 grains at 33 hours were absorbed into one grain after 180 hours. If pores shrank rapidly when encountered by the migrating boundaries of the growing grains, it would be expected that the pore densities after 33, 91, and 180 hours of heating would be in the ratio of 1:0.19:0.07, respectively, assuming a uniform pore distribution inside each grain. The experimentally-measured ratios were 1:0.23:0.04, respectively. Thus, it appears that essentially all pore removal occurred as a result of rapid disappearance of pores on grain boundaries. This conclusion is reinforced by observations of pore clusters during the experiment. Such clusters appeared to maintain a constant number of pores in a wide range of sizes throughout the experiment, indicating that gas flow between pores inside grains and from these pores to grain boundaries was negligible.

The qualitative picture of the mechanism of pore elimination caused by grain boundary migration is illustrated in Figure 14. In Figure 14A, it is assumed that there is a uniform distribution of equal-sized, spherical pores in all grains and that pores on grain boundaries are spherical. Some grains, having less than six sides in cross-section,

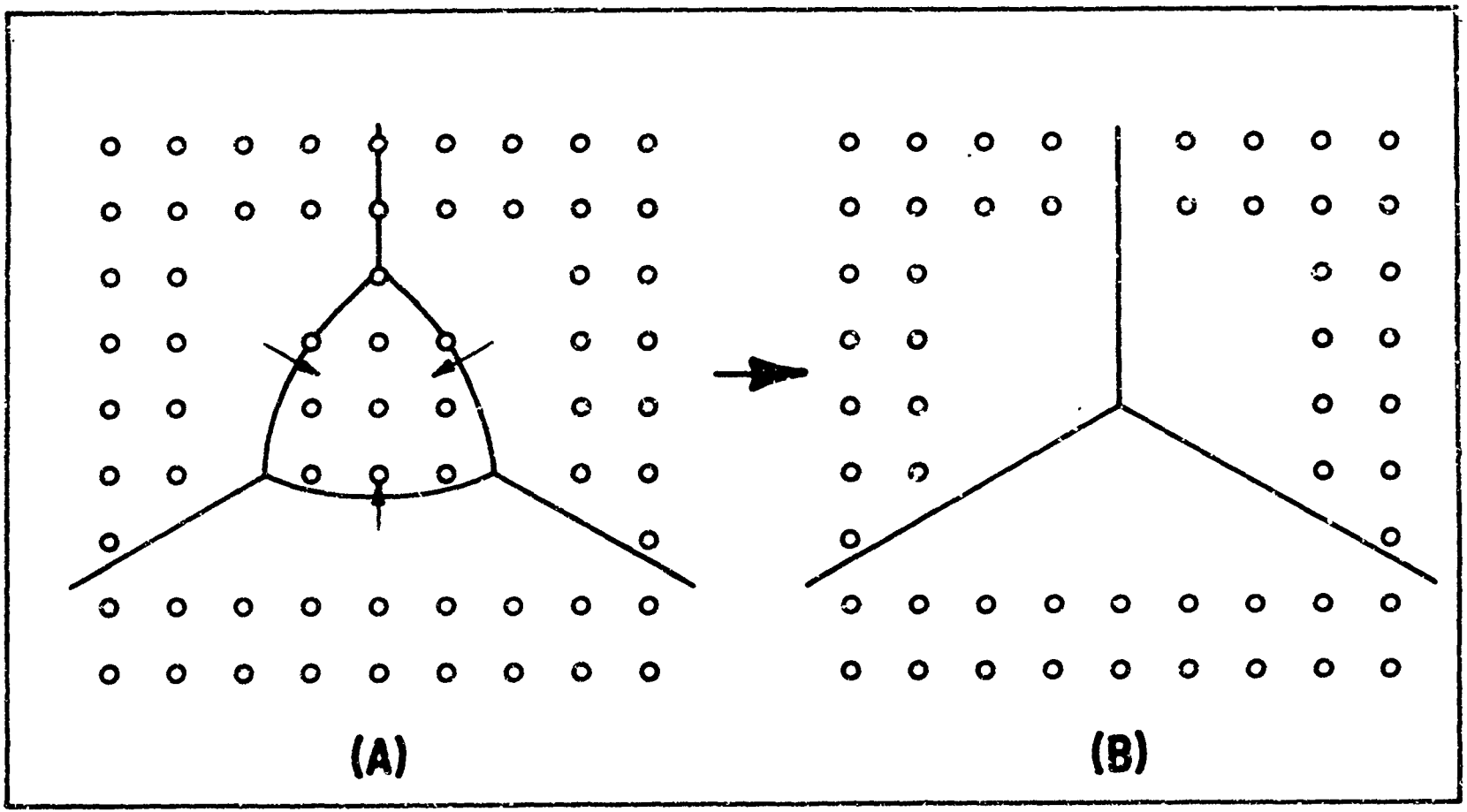

Figure 14 Qualitative mechanism of pore elimination by grain boundary movement. (A) Spherically-shaped pores, located primarily inside grains, will become relocated on a grain boundary of a shrinking grain. Arrows indicate the movement of grain boundaries towards their center of curvature. (B) Pore elimination caused by rapid shrinkage of pores on migrating grain boundaries during grain disappearance or grain growth.

E. Kinetics of Pore Disappearance...(continued)

shrink by the migration of their boundaries toward the center of curvature during grain growth. In this process, pores located inside a shrinking grain eventually meet a grain boundary and rapidly disappear. After the 3-sided grain disappears in Figure 14B, there is a pore-free region in the vicinity of the resulting triple point. Those pores which do not encounter a migrating grain boundary remain relatively unchanged in size and number.

The observations on pore disappearance at grain boundaries also imply that volume diffusion is not the primary mechanism by which such pores lost hydrogen gas to the boundary. The ratio of the final to initial heating times in this experiment is equal to about six, and the results given by theoretical calculations[2] indicate that considerable shrinkage of the pores inside grains should have occurred in this time if the pores on boundaries had disappeared by volume diffusion. Since this did not happen, and since all the observations indicate that the rate of shrinkage of pores on boundaries was much faster, perhaps by an order of magnitude or more, than the values calculated for equivalent pores inside grains, one is led to conclude that some other mechanism besides normal volume diffusion must have dominated the shrinkage of such pores. A possible mechanism that would lead to rapid shrinkage of closed pores on grain boundaries is that of direct passage of gas into a grain boundary along its intersection with the pore. Shrinkage rate controlled by a grain-boundary diffusion mechanism has previously been proposed to be operating during the initial and intermediate stages of sintering.[3,4,5]

III. GRAIN-GROWTH KINETICS

Isothermal grain-growth measurements were made on compacts sintered for various times at 2000 and 2170°C in a dry hydrogen atmosphere (Figure 15). At the same time and temperature, the average grain size was larger in

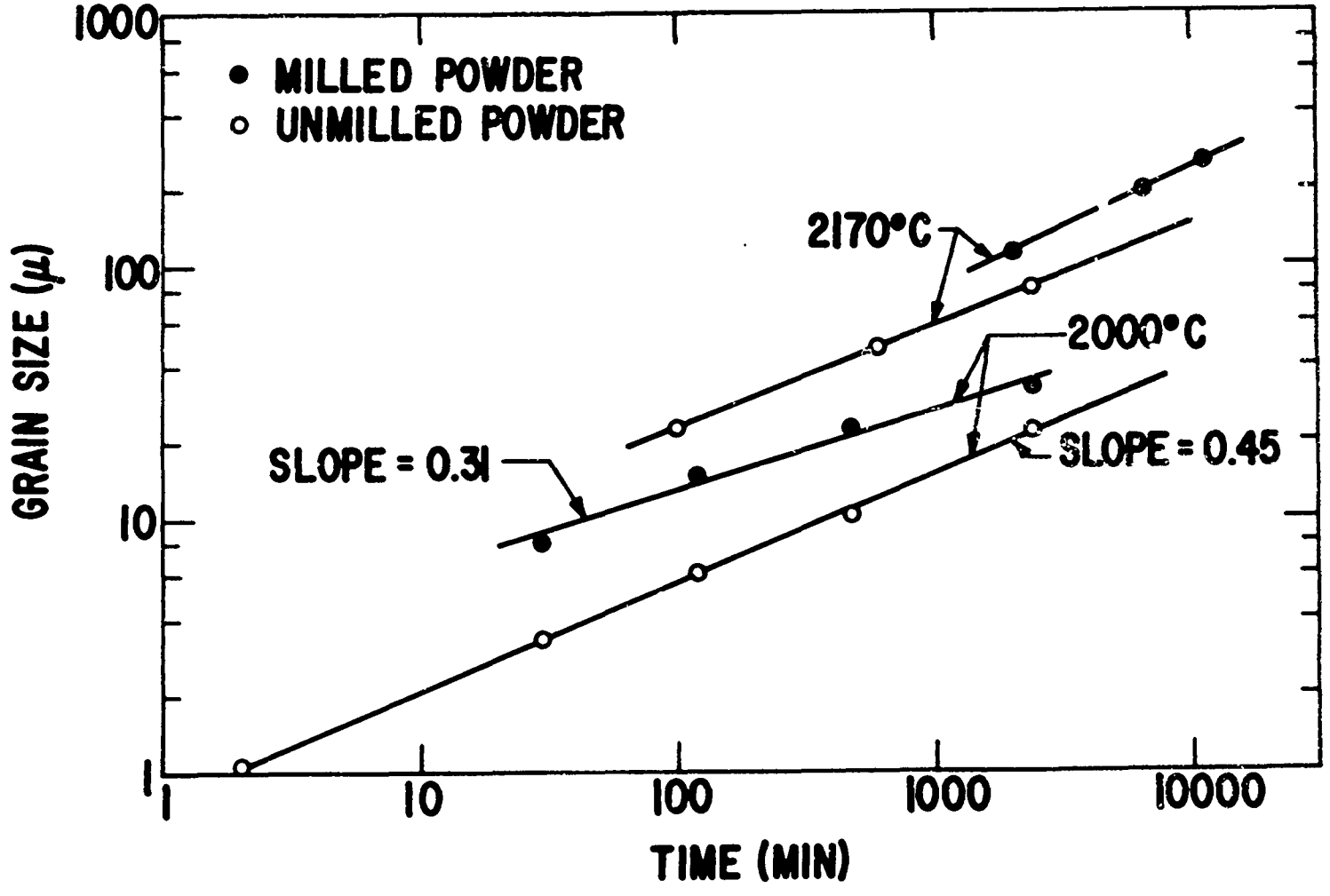

Figure 15 Grain size as a function of time and temperature for sintered Nd-doped Yttralox ceramic prepared from milled and unmilled powder.

sintered material prepared from powder milled in a rubber-lined mill than in sintered material prepared from unmilled powder. In addition, grain growth in specimens prepared from milled powder approximately followed a $t^{1/3}$ behavior whereas grain growth approximately followed a $t^{1/2}$ law for the unmilled material at 2000°C. These grain growth data in high-density, porous compacts can be understood by careful examination of the microstructure.

The microstructure of a compact prepared from unmilled powder and sintered for two hours at 2000°C is shown in Figure 16. This sintered material is characterized by a single solid phase, as confirmed by X-ray diffraction, and a closed-pore phase distributed primarily at three and four grain intersections. The location of these pores are indicative of grain growth controlled by pore migration but the square grain-growth kinetics found experimentally are not in agreement with cubic kinetics predicted from theory.[6] Square grain-growth kinetics has been previously found[7] for Y_2O_3 containing various amounts of ThO_2 in solid solution. In that work, it was reasonably well demonstrated that the addition of ThO_2 to Y_2O_3 inhibits grain growth during sintering by segregation of ThO_2 solute at grain boundaries, causing a decrease primarily in the grain boundary mobility. The major effect of the ThO_2 addition is to reduce grain-boundary mobility relative to that of pore mobility and thereby inhibit discontinuous grain growth. It appears then, that the ThO_2 addition, not pores, is responsible for controlling grain growth such that a square growth law is observed at 2000°C and 2170°C. Square grain-growth kinetics has been theoretically proposed for the effect of impurity drag on grain-boundary migration during continuous grain growth.[8]

A typical grain structure developed during the sintering of NDY material made from ball-milled powder is shown in Figure 17. In addition to the presence of pore clusters found inside grains, there was a highly-reflecting, solid second phase located at grain boundaries and grain intersections. By the use of a scanning electron microscope equipped with a solid-state X-ray detector, the second phase particles were found to be sulfur-rich (Figure 18).

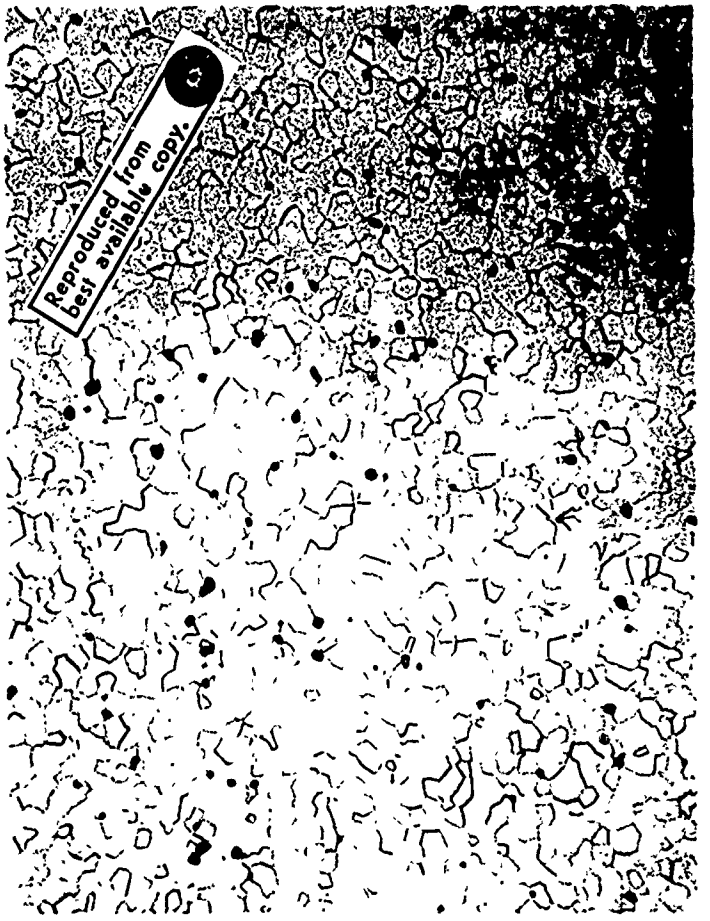

Figure 16 Microstructure of NDY ceramic illustrating pore-grain-boundary configuration. Specimen was prepared from unmilled powder and sintered for 2 hours at 2000°C in dry H_2. Reflected light, 500X.

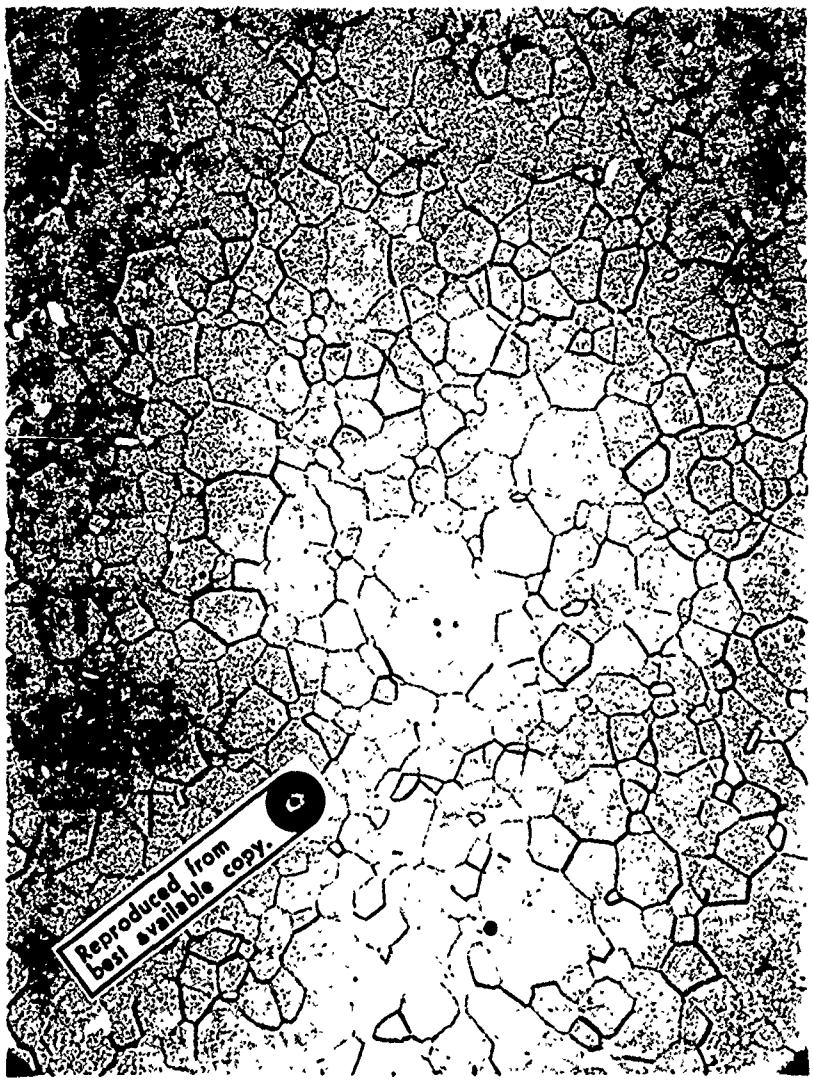

Figure 17 Grain structure in NDY ceramic sintered 2 hours at 2000°C in wet H_2. Note highly reflecting, sulfur-rich second phase at grain boundaries and grain intersections, and occasional pore cluster inside grains. Specimen was prepared from milled powder. Reflected light, 500X.

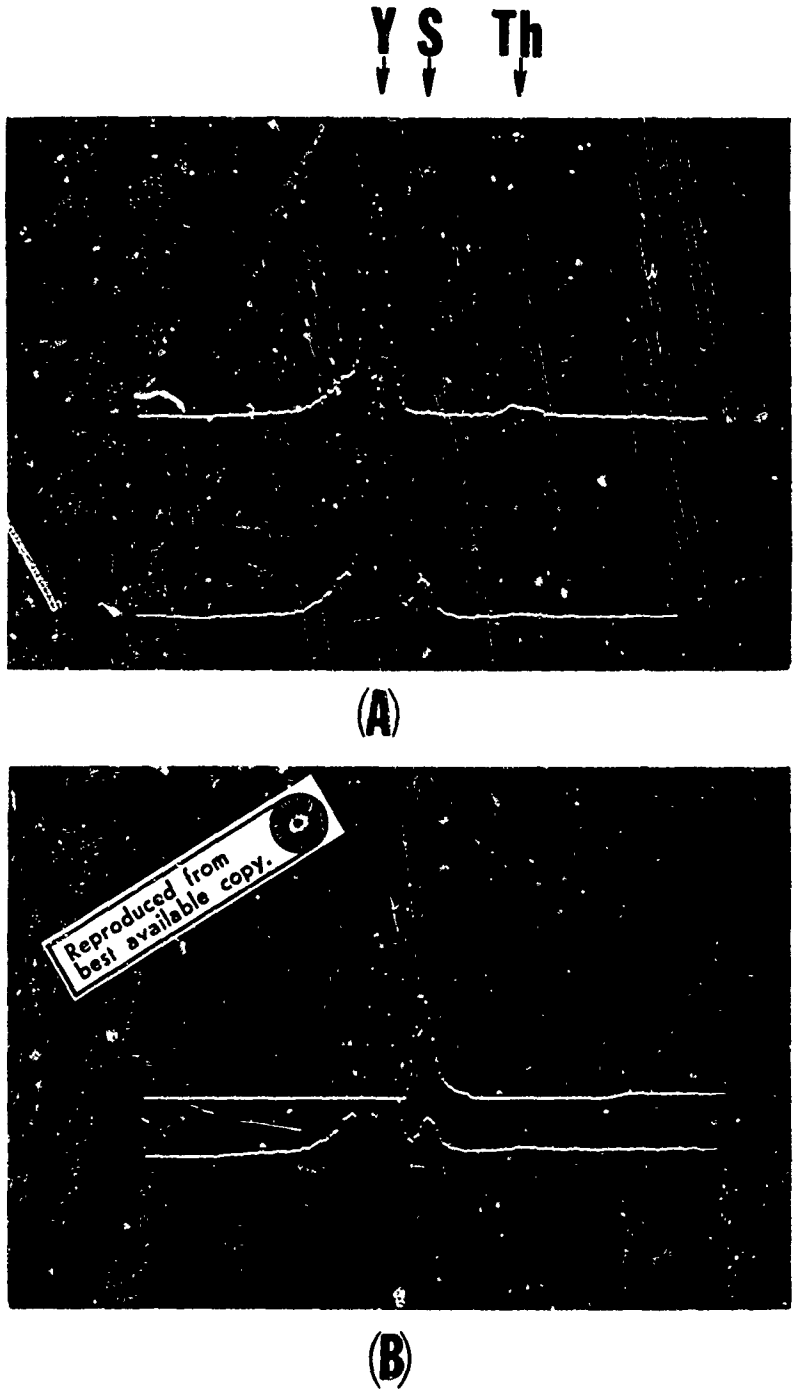

Figure 18 Solid-state x-ray spectra (on SEM) used to identify composition of second phase inclusions. (A) A NDY matrix grain (upper spectrum) and a second phase inclusion (lower spectrum). (B) Zinc sulfide sulfur standard (upper spectrum) and second phase inclusion (lower spectrum).

III. Grain-Growth Kinetics (continued)

Furthermore, the second-phase particles appeared to have a lower thorium content than the matrix grains. Sulfur contamination has been previously discussed[9] and is introduced into the powder by abrasion vulcanized-rubber lining of the ball mill during the milling operation.

The mechanism of grain growth in sulfur containing NDY ceramics at 2000°C is not exactly known but may be related to the inhibition of grain boundary movement by solid second-phase particles. The cubic relationship found for grain growth kinetics may be due to particle coalescence by a solution and reprecipitation phenomena similar to that described in the literature.[10] For the same time and atmosphere at 2000°C, sulfur-containing NDY ceramics have a larger average grain size because discontinuous grain growth occurs very early during the final stages of sintering and is evidenced by the presence of pore clusters entrapped inside grains (Figure 17). After the occurrence of discontinuous grain growth, there is a new generation of grains in which continuous grain growth occurs in the presence of second-phase particles. It is observed, however, that the solid second phase slowly disappears upon prolonged heating at 2000°C and at higher temperatures. In other words, sulfur is removed during the sintering process and causes the second phase to act as a transient phase during microstructural development. Although cubic grain-growth kinetics is observed in sulfur-containing NDY material over the time interval investigated at 2000°C, square-grain-growth kinetics are found for the same material at 2170°C for the time interval investigated. The reason for this observation is that at 2170°C there is no sulfur-rich, second phase that influences grain growth. This is supported by X-ray diffraction, reflected light, and transmitted light microscopy of polished sections.

IV. INFLUENCE OF POWDER PREPARATION ON ORANGE PEEL

'Orange peel' is a point-to-point variation in refractive index throughout a sintered NDY specimen prepared from unmilled powder produced by the oxalate process. It is thought to be related to chemical inhomogeneities

arising during powder preparation because orange peel can be reduced by screening or ball-milling the calcined powder before sintering. Both processing steps have a tendency to reduce compositional variations on a large scale in the starting powder, thus promoting a faster approach to chemical equilibrium during sintering. This optical phenomenon is not yet fully understood.

Two changes were made during powder preparation in order to determine if the amount of orange peel could be reduced in sintered material with the composition 89 mole % Y_2O_3, 10% ThO_2, and 1% Nd_2O_3. The first was to decrease the drip rate of the Y-Th-Nd salt solution into the oxalic acid bath from 100 to 50 drops/min and the second was to drip the oxalic acid bath into the Y-Th-Nd salt solution at a rate of 50 drops/min. Decreasing the drip rate from 100 to 50 drops/min caused no noticeable change in the amount of orange peel in the sintered product. The reverse precipitation procedure gave rise to a "grinding" noise at the bottom of the glass beaker used during the experiment. Sintered material prepared from this unmilled, calcined powder always contained a solid, second phase which was thoria-rich. Second-phase particles as large as 75μ, illustrated in Figure 19, could be found in material sintered for 57 hours at 2170°C in dry H_2. This second phase must have originated from the formation of thoria-rich agglomerates during the precipitation step. In addition, sintered material contained a considerable amount of orange peel.

Apparently, it is difficult to control orange peel by changing the precipitation rate by dripping the Y-Th-Nd salt solution into the oxalic acid bath or by the reverse precipitation procedure. Therefore, the Y-Th-Nd salt solution will be dripped into the oxalic acid bath at a rate between 50 and 100 drops/min and orange peel will be continued to be minimized or eliminated by a dry-milling operation, unless another approach is found which will produce a more chemically homogeneous starting powder.

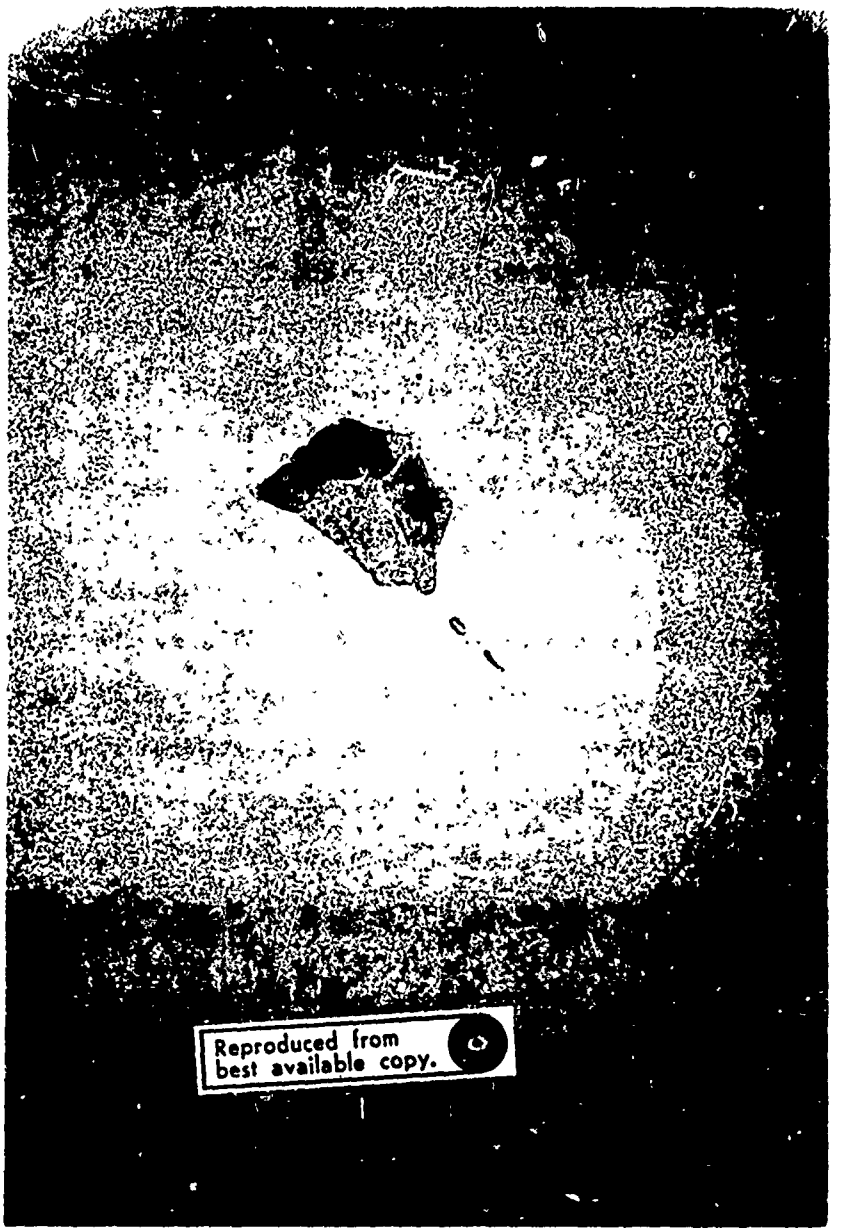

Figure 19 Thoria-rich, second phase particles found in sintered NDY ceramics prepared from an unfavorable starting powder. Specimen sintered for 57 hours at 2170°C, 240X.

V. OPTICAL MEASUREMENTS

A. Optical Quality

The optical quality of neodymium-doped Yttralox rods was compared to that of Nd-doped YAG single crystal and Nd-doped glass rods using a Twyman-Green interferometer. The YAG and glass rods were 7.62 cm in length and 0.625 cm in diameter, whereas the NDY rods were 7.62 cm in length and approximately 0.5 cm in diameter. These cylindrical rods had ends flat to $\lambda/10$, using Na light with λ = 5898Å, and ends parallel to ±2 arc seconds while maintaining perpendicularity to the rod axis.

The rods were examined with a double-pass Tywman-Green type interferometer operated with an He-Ne laser source (λ = 6328Å). Interferometer patterns for Nd-doped YAG rod (SIQ-Grade, Union Carbide), Nd-doped glass rod (ED-2 Laser glass, Owens Illinois) and Nd-doped Yttralox rod (YTC 13-4) are shown in Figure 20. The optical quality, determined by fringe count, of the NDY rod was comparable to that of the presently available YAG rod, about 1 fringe across the diameter of the rod, but not as good as glass which has approximately 1/5 fringe across the diameter. Glass rods of this size will normally exhibit no distortion except that introduced by imperfect finishing of the rod ends. The majority of Yttralox rods examined exhibited about 1 to 3 fringes of a random nature across the rod diameter whereas the interference pattern for YAG was somewhat non-uniform.

B. Spectral Transmittance

The spectral transmittance of Yttralox ceramic (90 mole % Y_2O_3 + 10% ThO_2) that is neodymium-free, including surface reflection losses, is shown in Figure 21. For a plate 3-1/2 mm thick, the short wavelength cut-on and long wavelength cut-off are approximately 1/4 and 9μ, respectively. Two surfaces reflect about 19% of incident radiation at a wavelength of about 1μ (refractive index ≈ 1.9). Transmission is

Figure 20 Twymann-Green interferometer patterns for (A) laser glass, (B) Nd-doped YAG and (C) Nd-doped Yttralox. Patterns show fringes in rods and visible background fringes.

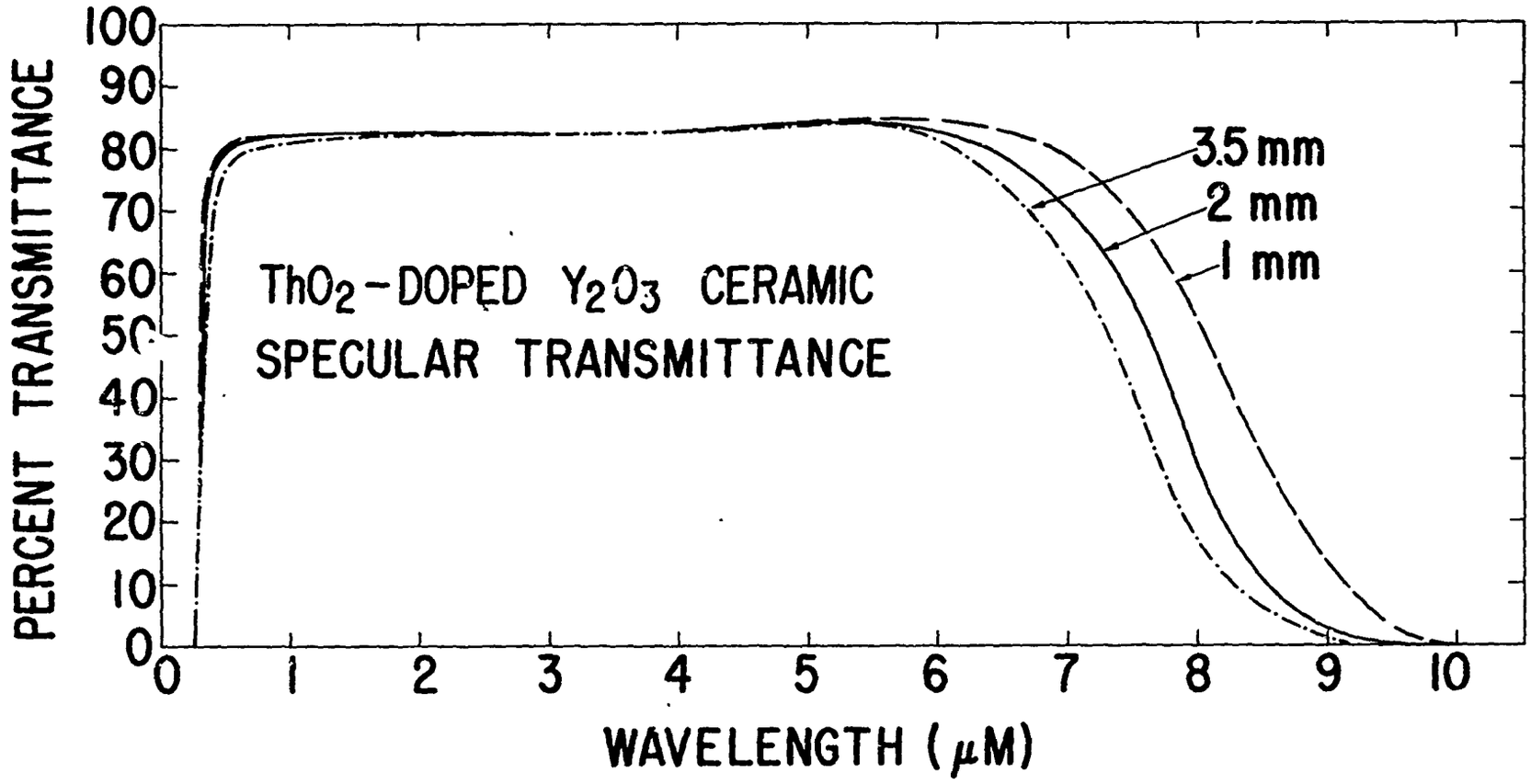

Figure 21 Specular transmittance of Nd-free Yttralox ceramic of various thicknesses.

B. Spectral Transmittance (continued)

greater than 80% between 0.75 and 6μ and appears to be relatively independent of sample thickness over the range of thicknesses examined in the wavelength region of 1.5 to 5.5μ. This means that the optical loss coefficient, which measures the attenuation of the light beam due to absorption and scattering, is low. The fact that there is high transmittance from the visible to the middle infrared region of the electromagnetic spectrum makes Yttralox ceramic suitable for visually aligning long wavelength detectors behind infrared transmitting windows, promising as a laser host material for the neodymium wavelength region of 1.07μ, and desirable for a variety of optical applications at high temperatures because of its high melting point (>2220°C).

C. Large-Angle Scattering Losses and Laser Thresholds

An attempt was made to determine if the measurement of large-angle scattering loss is a reliably quick method of qualitatively selecting NDY rods of good and poor optical quality. Large-angle scattering losses were measured on each lasing-quality rod at 6328Å relative to an Nd-doped glass rod (Owens Illinois, ED2 laser glass) in an integrating sphere photometer.

Laser threshold measurements, although more time-consuming, readily determined the degree of optical perfection exhibited by the laser rod. Laser measurements were carried out in a pump cavity which consisted of a 2.54 cm diameter, silvered, cylindrical reflector 5.62 cm in length. The flash lamp and laser rod were located symmetrically with respect to the center of the cylinder and spaced 0.95 cm apart. The flashlamp was a 4 mm bore, Xenon lamp with a 7.62 cm arc length, of which only 5.62 cm was utilized in pumping the laser rod. The lamp was energized by a 50μf capacitor bank that produced a pump-pulse duration of 150 microseconds. A Schott yellow glass filter was located between the flashlamp and the laser rod to absorb pump radiation of wavelengths shorter than 5000Å. Filtering is required to prevent solarization of

C. Large-Angle Scattering Losses...(continued)

the Yttralox material. The laser resonant cavity consisted of two dielectric mirrors, one flat and one with a radius of curvature of two meters, spaced 20 cm apart. Laser threshold energy was detected by the "spiking" characteristics commonly observed in pulsed, solid-state lasers and defined as the pump energy required to produce spiking at a given output mirror reflectivity.

Values of (relative) scattering loss, laser threshold, and porosity, the only optical defect which was quantitatively measured, for NDY rods about 7.62 cm in length and about 5 mm in diameter are given in Table I.

TABLE I

LARGE-ANGLE SCATTERING LOSS, LASER THRESHOLD, AND POROSITY FOR NDY RODS RELATIVE TO LASER GLASS

Specimen	Porosity	Relative Scattering Loss	Threshold (joules) at 95% R
OI, ED2 Glass	≈0	≈0	9
YTC 11-3	3.2×10^{-6}	4.9	30
YTS 12-1	3.3×10^{-7}	3.1	21
YTC 13-4B	8.2×10^{-7}	1.4	16
YTC 13-4A	8.2×10^{-7}	1.0	8
YTC 15-2	9.5×10^{-6}	5.8	36
YTC 16-3	1.2×10^{-5}	4.5	38
YTC 16-7	3.5×10^{-5}	2.3	>100

Powder composition, processing and sintering time at temperature are now described for the NDY rods so that the data presented in Table I can be understood in greater detail. Unless otherwise specified, the NDY rods were synthesized in the same manner. The nominal composition of the NDY rods was 89 mole % Y_2O_3, 10% ThO_2, and 1% Nd_2O_3, except YTC 15-2 rod whose composition was 92% Y_2O_3, 7% ThO_2, and 1% Nd_2O_3.

C. Large-Angle Scattering Losses...(continued)

Examination of YTC 15-2 rod by transmitted light microscopy showed no major difference except in porosity. All NDY rods were prepared from ball-milled powder except YTC 16-7 rod. In addition to porosity, YTC 16-7 rod contained a substantial amount of orange peel as evidenced by transmitted light microscopy and the naked eye. Finally, NDY rods were sintered for about 100 hours at 2170°C except YTC 11-3 rod, which was sintered for only 58 hours. Microscopic examination of this rod revealed the presence of a small amount of a sulfur-rich, solid second phase located at grain boundaries and grain intersections. This sulfur-rich second phase was absent in other rods. YTC 13-4A rod is discussed later in the text.

There are, then, several sources of light-scattering centers in NDY ceramics. The most common scattering defects observed microscopically are porosity, solid second phase, and orange peel. The presence of submicroscopic scattering defects is discussed later. It is difficult to correlate large-angle scattering loss with porosity (or volume fraction of pores) or the amount of second phase because particle number, size, distribution, and shape are important in understanding the magnitude of light-scattering losses. Since most pores in all samples are greater in size than the wavelength of light in the material (i.e., $> 0.33\mu$), such pores scatter light strongly in the forward direction and most of this scattered light is not detected by the integrating sphere technique. Hence, (relative) large-angle scattering losses, measured by an integrating sphere photometer, appear to be very difficult to interpret and, with the current experimental setup, this method probably cannot readily screen out good and poor quality laser rods currently produced.

Laser threshold energy, as well as active loss coefficient and lasing efficiency, which are discussed later, is an excellent method of assessing the overall optical quality of a laser rod. In reference to

C. Large-Angle Scattering Losses...(continued)

Table I, YTC 12-1 and YTC 13-4B rods have low porosity and also relatively low laser thresholds, whereas YTC 16-3 and YTC 16-7 rods have the high porosities and high threshold values. YTC 16-7 rod contains about 3 times as much porosity as YTC 16-3 and has a laser threshold greater than 100 joules because, in addition to porosity, this specimen contains a considerable amount of orange peel. Another interesting comparison is that YTC 15-2 and YTC 16-3 have nearly the same porosity (primarily in the form of pore clusters) and nearly the same laser thresholds, although YTC 15-2 rod contains 7 mole % ThO_2. Changing the thoria content from 10 to 7 mole % apparently causes little change in the fluorescent behavior of the Nd^{3+} ions in the vicinity of the emitting wavelength at 1.07μ. There appears to be, therefore, a relationship between porosity and laser threshold, even though the sintered rods have somewhat different pore size distributions. This is understandable because the majority of pores in all NDY rods are of a size that is comparable to or larger than the wavelength of light in the transmitting medium. The relationship for scattering by large particles, $\frac{\pi dm}{\lambda} >> 1$, is approximately valid; and consequently, the scattering efficiency for such particles is relatively independent of wavelength (λ). The relative refractive index of the pore to the transmitting medium is (m).

D. Active Loss Coefficient and Laser Output Efficiency

The attenuation of a beam of parallel monochromatic radiation as it propagates through a laser rod can be determined by active laser measurements. The "active" attenuation coefficient or material loss coefficient is determined from laser threshold energy for different output mirror reflectivities. Laser threshold can be given by the condition

$$\frac{1}{R_1 R_2} = \exp[-(\sigma n - \gamma)2\ell] \qquad (1)$$

D. Active Loss Coefficient...(continued)

where R_1 and R_2 are the mirror reflectives, σ is the stimulation cross section, n the inversion density of electrons caused by the pump radiation, γ the active loss coefficient of the material, and ℓ the length of the laser rod. If $\frac{1}{R_1 R_2}$ is plotted as a function of threshold energy on a semilogarithmic scale and extrapolated to zero pump energy or threshold energy, then for n = o, the intercept along the ordinate gives

$$\ell n \frac{1}{R_1 R_2} = -\gamma 2\ell \quad . \tag{2}$$

The value of γ can be determined from the above equation. This type of plot is shown in Figure 22 for several NDY rods 7.62 cm in length and Nd-doped glass rod 15.2 cm in length. Calculated active loss coefficients are listed in Table II.

TABLE II

ACTIVE LOSS COEFFICIENT FOR NDY RODS AND Nd-DOPED GLASS ROD

Specimen	Active Loss Coefficient
YTC 13-4B	4.9%/cm
YTC 13-4A	2.6%/cm
YTC 12-1	5.4%/cm
YTC 11-3	6.9%/cm
OI ED-2 Glass	0.76%/cm

Laser output was measured as a function of input energy in the previously described pump cavity. The output mirror used had a reflectivity of 80%. Results of these measurements are shown in Figure 23 for NDY rods with high optical perfection and for Nd-doped glass used as a reference material. Since the NDY rods were smaller in diameter than the glass rod (6.35 mm diameter), data plotted in Figure 23 were normalized with respect to the diameter of the glass rod because for larger rod diameters,

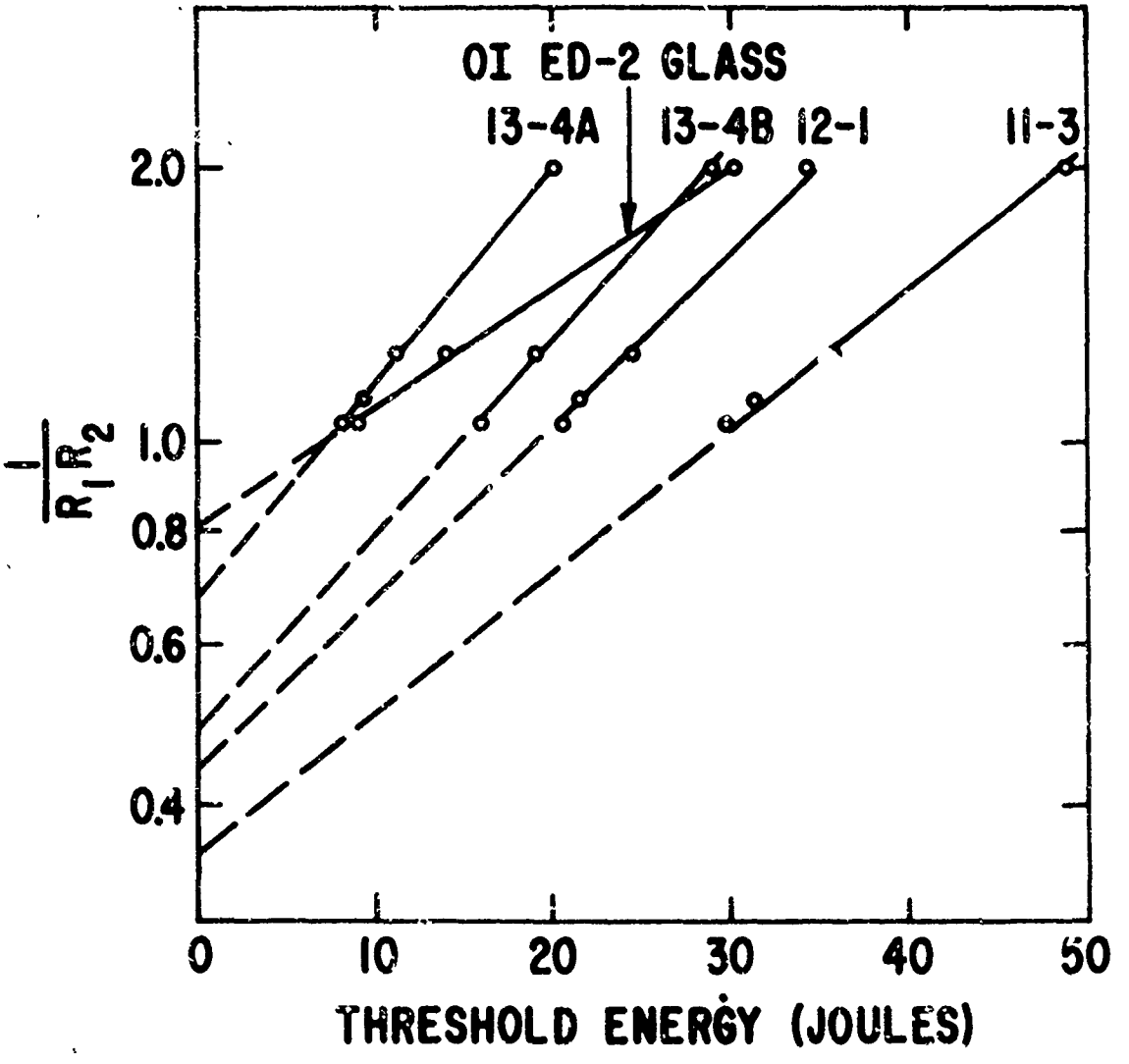

Figure 22 Effect of output mirror reflectivity (R_2) on the pump energy required for laser threshold. Mirror reflectivity, R_1, was ≈ 1.

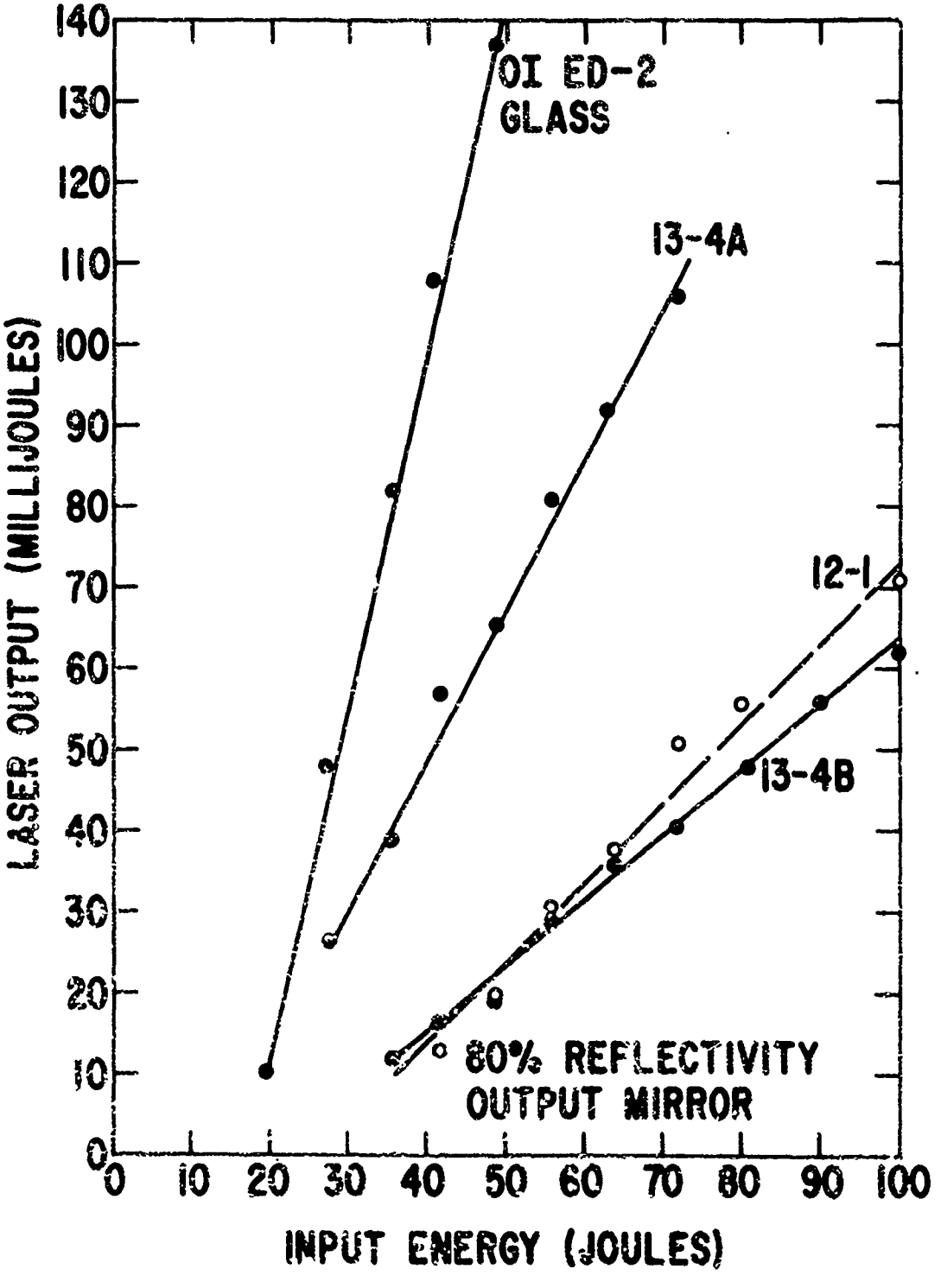

Figure 23 Energy output versus energy input for several rods. Output mirror reflectivity 80%.

D. Active Loss Coefficient...(continued)

there is increased surface area available for capture of flashlamp radiation. In this way, a direct comparison can be made between these data and slope efficiencies recorded in Table III.

TABLE III

LASER SLOPE EFFICIENCY FOR NDY RODS AND Nd-DOPED GLASS ROD

Specimen	Slope Efficiency (%)
YTC 13-4B	0.081
YTC 13-4A	0.19
YTC 12-1	0.098
OI ED-2 glass	0.44

The data in Table II and Table III show that Nd-doped Yttralox rods YTC 13-4B and YTC 12-1, both of which had identical powder preparation, processing, and thermal cycling conditions, have nearly the same active loss coefficient (i.e., $\approx$ 5%/cm) and laser slope efficiency (i.e., $\sim$ 0.09%). On the other hand, laser glass has an active loss coefficient and slope efficiency of 0.76%/cm and 0.44%, respectively. Glass is, therefore, about a half an order of magnitude superior in laser performance than the two NDY rods mentioned. YTC 11-3 rod has a higher active loss coefficient than YTC 13-4B and YTC 12-1 rods, probably because it has higher porosity and, in addition, contains a small amount of solid second phase which scatters light.

An experiment was carried out to determine if the cooling cycle influenced the optical quality and lasing performance of Nd-doped Yttralox ceramic. The cooling curve for YTC 13-4B rod cooled under automatic programming conditions in a Brew[11] furnace is given in Figure 24. After making measurements of lasing threshold, active loss coefficient, and laser output efficiency, the same rod was heated to

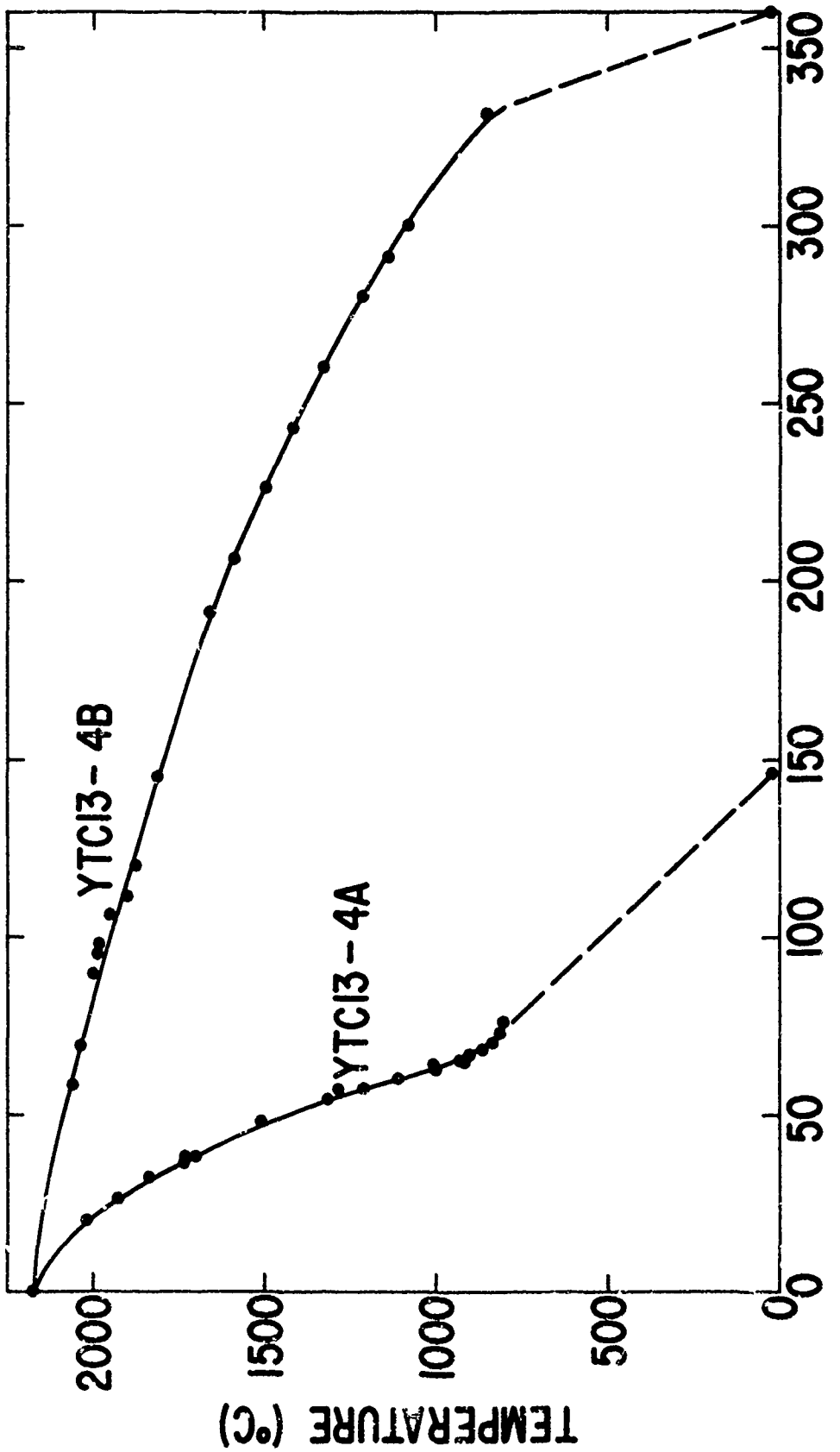

Figure 24 Cooling curves for YTC13-4 rod. Dashed part of the curve is an approximation.

D. Active Loss Coefficient...(continued)

the sintering temperature of 2170°C, equilibrated for two hours only so that very little sintering, if any, occurred, and then cooled much faster to room temperature. This rapidly-cooled specimen is labeled YTC 13-4A in Figure 24. Specimen preparation for lasing measurements was identical to that of YTC 13-4B and all other laser rods tested.

Active lasing measurements for YTC 13-4A recorded in Tables I, II, and III, and in Figure 23 showed that, in comparison to those values for YTC 13-4B rod which was cooled slowly to room temperature, the lasing threshold was reduced by 51%, active loss coefficient decreased by 53% and the lasing slope efficiency increased by 234%. These results indicate that the faster cooling cycle has a pronounced effect on the laser performance. A direct comparison of active lasing measurements for YTC 13-4B, YTC 13-4A, and laser glass is given in Table IV. Note that YTC 13-4A rod has achieved a lower threshold value than that of laser glass, and a lasing slope efficiency approximately 43% of that of laser glass.

TABLE IV

ACTIVE LASER MEASUREMENTS FOR NDY AND LASER GLASS RODS

Sample	Threshold at 95% R	Active Loss Coefficient	Slope Efficiency
YTC 13-4B	16	4.9%/cm	0.081%
YTC 13-4A	8	2.6%/cm	0.19%
OI, ED2 Glass	9	0.76%/cm	0.44%

The reason for the large improvement in lasing characteristics of the Nd-doped Yttralox rod by the fast-cooling technique is not yet clearly established but is thought to be related to submicroscopic precipitation or ordering effects. Neodymium-doped Yttralox is a polycrystalline ceramic composed of a solid solution of 89 mole % Y_2O_3, 10% ThO_2, and 1% Nd_2O_3. Rapid cooling probably causes a retention of

D. Active Loss Coefficient...(continued)

the high-temperature, disordered solid-solution and prevents growth of ordered zones or extended defects at lower temperatures. Such extended defects represent changes in structure and composition which can produce fluctuations of local refractive index that scatter light. Extended defects, by their very nature, are substructures which are coherent with the matrix and are extremely difficult to detect by conventional methods. For example, extended defects in stabilized zirconia,[12] which control the electrical resistivity behavior at relatively high temperatures, could not be observed with conventional microscopic or X-ray methods but could be observed with neutron diffraction and single-crystal X-ray diffraction.

Further support for the presence of submicroscopic scattering centers in NDY materials can be deduced from preliminary results obtained by ultramicroscopy and theoretical light-scattering calculations. It can be shown that pores alone cannot account for the high-loss coefficients (≈5%/cm) found in slow-cooled NDY rods. If the absorption coefficient is assumed to be much smaller than the scattering coefficient at the lasing wavelength of 1.07μ, then there must be submicroscopic scattering centers in the NDY material. During the third year's contract, more direct and more quantitative evidence will be sought to identify submicroscopic defects.

VI. REFERENCES

1. F. Thummler and W. Thoma, "The Sintering Process", Met. Reviews, 1 69-108 (1967).
2. J. H. Rosolowski and C. Greskovich, "Analysis of Pore Shrinkage by Volume Diffusion During Final Stage Sintering", submitted to J. Appl. Physics.

VI. References (continued)

3. D. L. Johnson, "Sintering and Related Phenomena", Conference Proceedings, Notre Dame U., June 1965, Gordon and Breach, New York 1967.

4. D. L. Johnson, "A General Model for the Intermediate Stage of Sintering", J. Amer. Ceram. Soc., 53 (10) 574-77 (1970).

5. H. U. Anderson, "Initial Sintering of $BaTiO_3$ Compacts," J. Amer. Ceram. Soc., 48 (3) 118-21 (1965).

6. W. D. Kingery and B. Francois, "Grain Growth in Porous Compacts," J. Amer. Ceram. Soc., 48 [10] 546-47 (1965).

7. P. J. Jorgensen and R. C. Anderson, "Grain-Boundary Segregation and Final-Stage Sintering of Y_2O_3," J. Amer. Ceram. Soc., 50 (11) 553-58 (1967).

8. R. J. Brook, "The Impurity-Drag Effect and Grain Growth Kinetics," Scripta Met., 2 375-78 (1968).

9. C. Grenkovich and K. N. Woods, "Yttralox Ceramic Laser," Annual Report, 44 pp, (June 1970-May 1971), July 1971.

10. I. M. Lifshits and V. V. Slezov, "Kinetics of Diffusive Decomposition of Supersaturated Solid Solutions," Soviet Physics JETP (English Transl.), 35 (8) 331-39 (1959).

11. Richard D. Brew Co., Inc., Concord, New Hampshire.

12. R. E. Carter and W. L. Roth, General Electric Corporate Research and Development Report No. 67-C-308, 1967.